Doc Code: **TR.PROV**
Document Description: Provisional Cover Sheet (SB16)

PTO/SB/16 (11-08)
Approved for use through 01/31/2014 OMB 0651-0032
U.S. Patent and Trademark Office: U.S. DEPARTMENT OF COMMERCE

Provisional Application for Patent Cover Sheet

This is a request for filing a PROVISIONAL APPLICATION FOR PATENT under 37 CFR 1.53(c)

Inventor(s)

Inventor 1 — Remove

Given Name	Middle Name	Family Name	City	State	Country
Eric		Van Stryland	Cape Canaveral	FL	US

Inventor 2 — Remove

Given Name	Middle Name	Family Name	City	State	Country
David	J.	Hagan	Oviedo	FL	US

All Inventors Must Be Listed – Additional Inventor Information blocks may be generated within this form by selecting the **Add** button. — Add

Title of Invention	OPTICAL SENSING METHOD, APPARATUS, AND APPLICATIONS
Attorney Docket Number (if applicable)	1335P011

Correspondence Address

Direct all correspondence to (select one):

◉ The address corresponding to Customer Number	◯ Firm or Individual Name
Customer Number	11720

The invention was made by an agency of the United States Government or under a contract with an agency of the United States Government.

◯ No.

◉ Yes, the name of the U.S. Government agency and the Government contract number are:

US Army 50372 CHMUR; DARPA ZOE W31R4Q-09-1-0012

Doc Code: **TR.PROV**
Document Description: Provisional Cover Sheet (SB16)

PTO/SB/16 (11-08)
Approved for use through 01/31/2014 OMB 0651-0032
U.S. Patent and Trademark Office: U.S. DEPARTMENT OF COMMERCE

Entity Status

Applicant claims small entity status under 37 CFR 1.27

- (●) Yes, applicant qualifies for small entity status under 37 CFR 1.27
- ( ) No

Warning

Petitioner/applicant is cautioned to avoid submitting personal information in documents filed in a patent application that may contribute to identity theft. Personal information such as social security numbers, bank account numbers, or credit card numbers (other than a check or credit card authorization form PTO-2038 submitted for payment purposes) is never required by the USPTO to support a petition or an application. If this type of personal information is included in documents submitted to the USPTO, petitioners/applicants should consider redacting such personal information from the documents before submitting them to USPTO. Petitioner/applicant is advised that the record of a patent application is available to the public after publication of the application (unless a non-publication request in compliance with 37 CFR 1.213(a) is made in the application) or issuance of a patent. Furthermore, the record from an abandoned application may also be available to the public if the application is referenced in a published application or an issued patent (see 37 CFR1.14). Checks and credit card authorization forms PTO-2038 submitted for payment purposes are not retained in the application file and therefore are not publicly available.

Signature

Please see 37 CFR 1.4(d) for the form of the signature.

Signature	/William Greener/			Date (YYYY-MM-DD)	2011-11-23
First Name	William	Last Name	Greener	Registration Number (If appropriate)	38165

This collection of information is required by 37 CFR 1.51. The information is required to obtain or retain a benefit by the public which is to file (and by the USPTO to process) an application. Confidentiality is governed by 35 U.S.C. 122 and 37 CFR 1.11 and 1.14. This collection is estimated to take 8 hours to complete, including gathering, preparing, and submitting the completed application form to the USPTO. Time will vary depending upon the individual case. Any comments on the amount of time you require to complete this form and/or suggestions for reducing this burden, should be sent to the Chief Information Officer, U.S. Patent and Trademark Office, U.S. Department of Commerce, P.O. Box 1450, Alexandria, VA 22313-1450. DO NOT SEND FEES OR COMPLETED FORMS TO THIS ADDRESS. **This form can only be used when in conjunction with EFS-Web. If this form is mailed to the USPTO, it may cause delays in handling the provisional application.**

Privacy Act Statement

The Privacy Act of 1974 (P.L. 93-579) requires that you be given certain information in connection with your submission of the attached form related to a patent application or paten. Accordingly, pursuant to the requirements of the Act, please be advised that : (1) the general authority for the collection of this information is 35 U.S.C. 2(b)(2); (2) furnishing of the information solicited is voluntary; and (3) the principal purpose for which the information is used by the U.S. Patent and Trademark Office is to process and/or examine your submission related to a patent application or patent. If you do not furnish the requested information, the U.S. Patent and Trademark Office may not be able to process and/or examine your submission, which may result in termination of proceedings or abandonment of the application or expiration of the patent.

The information provided by you in this form will be subject to the following routine uses:

1. The information on this form will be treated confidentially to the extent allowed under the Freedom of Information Act (5 U.S.C. 552) and the Privacy Act (5 U.S.C 552a). Records from this system of records may be disclosed to the Department of Justice to determine whether disclosure of these records is required by the Freedom of Information Act.
2. A record from this system of records may be disclosed, as a routine use, in the course of presenting evidence to a court, magistrate, or administrative tribunal, including disclosures to opposing counsel in the course of settlement negotiations.
3. A record in this system of records may be disclosed, as a routine use, to a Member of Congress submitting a request involving an individual, to whom the record pertains, when the individual has requested assistance from the Member with respect to the subject matter of the record.
4. A record in this system of records may be disclosed, as a routine use, to a contractor of the Agency having need for the information in order to perform a contract. Recipients of information shall be required to comply with the requirements of the Privacy Act of 1974, as amended, pursuant to 5 U.S.C. 552a(m).
5. A record related to an International Application filed under the Patent Cooperation Treaty in this system of records may be disclosed, as a routine use, to the International Bureau of the World Intellectual Property Organization, pursuant to the Patent Cooperation Treaty.
6. A record in this system of records may be disclosed, as a routine use, t o a n other federal agency for purposes of National Security review (35 U.S.C. 181) and for review pursuant to the Atomic Energy Act (42 U.S.C. 218(c)).
7. A record from this system of records may be disclosed, as a routine use, to the Administrator, General Services, or his/her designee, during an inspection of records conducted by GSA as part of that agency's responsibility to recommend improvements in records management practices and programs, under authority of 44 U.S.C. 2904 and 2906. Such disclosure shall be made in accordance with the GSA regulations governing inspection of records for this purpose, and any other relevant (i.e., GSA or Commerce) directive. Such disclosure shall not be used to make determinations about individuals.
8. A record from this system of records may be disclosed, as a routine use, to the public after either publication of the application pursuant to 35 U.S.C. 122(b) or issuance of a patent pursuant to 35 U.S.C. 151. Further, a record may be disclosed, subject to the limitations of 37 CFR 1.14, as a routine use, to the public if the record was filed in an application which became abandoned or in which the proceedings were terminated and which application is referenced by either a published application, an application open to public inspection or an issued patent.
9. A record from this system of records may be disclosed, as a routine use, to a Federal, State, or local law enforcement agency, if the USPTO becomes aware of a violation or potential violation of law or regulation.

Attorney Docket No. 1335P011

UNITED STATES PROVISIONAL PATENT APPLICATION

Optical Sensing Method, Apparatus, and Applications

INVENTOR
Eric Vanstryland
David J. Hagan

Optical Sensing Method, Apparatus, and Applications

The attached PROV_DISC_1, PROV_DISC_2, and PROV_DISC_3 provide a non-limiting, exemplary description of the embodied invention and form an integral part of applicant's provisional application.

This work was supported in part by the US Army Research Office (grant no. 50372-CHMUR) and the DARPA ZOE program (grant no. W31R4Q-09-1-0012). The government has rights in the invention.

Non-limiting, exemplary embodiments of the invention include:

1. An optical sensing method comprising optically pumping a semiconductor material through irradiation with and absorption of a first photon having a first energy to enhance sensitivity of the semiconductor material for absorption of a second photon having a second energy different than the first energy.

2. The method of claim 1 wherein at least one of the first energy and the second energy is in the near infrared to infrared region.

3. The method of claim 1 wherein the first energy is lower than the second energy.

4. The method of claim 1 wherein at least one of the first energy and the second energy is in a range from about 5 to about 20 percent of a bandgap of the semiconductor material.

5. The method of claim 1 wherein the first energy and the second energy differ by a factor of at least 5.

Extremely nondegenerate two-photon absorption in direct-gap semiconductors [Invited]

Claudiu M. Cirloganu, Lazaro A. Padilha, Dmitry A. Fishman, Scott Webster, David J. Hagan, and Eric W. Van Stryland*

CREOL: The College of Optics and Photonics, University of Central Florida, 4000 Central Florida Blvd, Orlando, FL, 32816, USA

**ewvs@creol.ucf.edu*

Abstract: Two-photon absorption (2PA) spectra with pairs of extremely nondegenerate photons are measured in several direct-gap semiconductors (GaAs, CdTe, ZnO, ZnS and ZnSe) using picosecond or femtosecond pulses. In ZnSe, using photons with a ratio of energies of ~12, we obtain a 270-fold enhancement of 2PA when comparing to the corresponding degenerate 2PA coefficient at the average photon energy $(\eta\omega_1 + \eta\omega_2)/2$. This corresponds to a pump photon energy of 8% of the bandgap. 2PA coefficients as large as 1 cm/MW are measured. Thus, by using two widely different wavelengths we are able to access the large 2PA observed previously only in narrow gap semiconductors. We also calculate the corresponding enhancement of nonlinear refraction, consisting of two-photon, AC-Stark and Raman contributions. The net effect is a smaller enhancement, but exhibits very large dispersion within the 2PA regime.

OCIS codes: (190.0190) Nonlinear optics; (300.6410) Spectroscopy, multiphoton; (190.7110) Ultrafast nonlinear optics.

References and links

1. J. A. Bolger, A. K. Kar, B. S. Wherrett, R. DeSalvo, D. C. Hutchings, and D. J. Hagan, "Nondegenerate two-photon absorption spectra of ZnSe, ZnS and ZnO," Opt. Commun. **97**(3–4), 203–209 (1993).
2. A. A. Said, M. Sheik-Bahae, D. J. Hagan, T. H. Wei, J. Wang, J. Young, and E. W. Van Stryland, "Determination of bound-electronic and free-carrier nonlinearities in ZnSe, GaAs, CdTe, and ZnTe," J. Opt. Soc. Am. B **9**(3), 405–414 (1992).
3. M. Sheik-Bahae, D. C. Hutchings, D. J. Hagan, and E. W. Van Stryland, "Dispersion of bound electron nonlinear refraction in solids," IEEE J. Quantum Electron. **27**(6), 1296–1309 (1991).
4. E. W. Van Stryland, M. A. Woodall, H. Vanherzeele, and M. J. Soileau, "Energy band-gap dependence of two-photon absorption," Opt. Lett. **10**(10), 490–492 (1985).
5. P. D. Olszak, C. M. Cirloganu, S. Webster, L. A. Padilha, S. Guha, L. P. Gonzalez, S. Krishnamurthy, D. J. Hagan, and E. W. Van Stryland, "Spectral and temperature dependence of two-photon and free-carrier absorption in InSb," Phys. Rev. B **82**(23), 235207 (2010).
6. B. S. Wherrett, "Scaling rules for multiphoton interband absorption in semiconductors," J. Opt. Soc. Am. B **1**(1), 67–72 (1984).
7. D. A. Fishman, C. M. Cirloganu, S. Webster, L. A. Padilha, M. Monroe, D. J. Hagan, and E. W. Van Stryland, "Sensitive mid-infrared detection in wide-gap semiconductors using extreme nondegenerate two-photon absorption," Nat. Photonics **5**(9), 561–565 (2011).
8. F. Urbach, "The long-wavelength edge of photographic sensitivity and of the electronic absorption of solids," Phys. Rev. **92**(5), 1324 (1953).
9. A. E. Rakhshani, "Study of Urbach tail, bandgap energy and grain-boundary characteristics in CdS by modulated photocurrent spectroscopy," J. Phys. Condens. Matter **12**(19), 4391–4400 (2000).
10. S. Keuleyan, E. Lhuillier, V. Brajuskovic, and P. Guyot-Sionnest, "Mid-infrared HgTe colloidal quantum dot photodetectors," Nat. Photonics **5**(8), 489–493 (2011).
11. A. Hayat, P. Ginzburg, and M. Orenstein, "Observation of two-photon emission from semiconductors," Nat. Photonics **2**(4), 238–241 (2008).
12. D. C. Hutchings, M. Sheik-Bahae, D. J. Hagan, and E. W. Stryland, "Kramers-Kronig Relations in Nonlinear Optics," Opt. Quantum Electron. **24**(1), 1–30 (1992).
13. F. T. Arecchi, E. O. Schulz-Dubois, M. L. Stitch, W. B. Colson, C. Pellegrini, and A. Renieri, Laser handbook. 1972, Amsterdam, New York: North-Holland Pub. Co.; American Elsevier Pub. Co. v. <1–6 >.

#153971 - $15.00 USD Received 6 Sep 2011; revised 24 Oct 2011; accepted 25 Oct 2011; published 28 Oct 2011

14. A. Bhaskar, G. Ramakrishna, Z. Lu, R. Twieg, J. M. Hales, D. J. Hagan, E. Van Stryland, and T. Goodson 3rd, "Investigation of two-photon absorption properties in branched alkene and alkyne chromophores," J. Am. Chem. Soc. **128**(36), 11840–11849 (2006).
15. D. C. Hutchings and E. W. V. Stryland, "Nondegenerate two-photon absorption in zinc blende semiconductors," J. Opt. Soc. Am. B **9**(11), 2065–2074 (1992).
16. J. M. Hales, D. J. Hagan, E. W. Van Stryland, K. J. Schafer, A. R. Morales, K. D. Belfield, P. Pacher, O. Kwon, E. Zojer, and J. L. Bredas, "Resonant enhancement of two-photon absorption in substituted fluorene molecules," J. Chem. Phys. **121**(7), 3152–3160 (2004).
17. H. D. Jones and H. R. Reiss, "Intense-field effects in solids," Phys. Rev. B **16**(6), 2466–2473 (1977).
18. D. C. Hutchings and B. S. Wherrett, "Theory of anisotropy of 2-photon absorption in zincblende semiconductors," Phys. Rev. B **49**(4), 2418–2426 (1994).
19. C. M. Cirloganu, P. D. Olszak, L. A. Padilha, S. Webster, D. J. Hagan, and E. W. V. Stryland, "Three-photon absorption spectra of zinc blende semiconductors: theory and experiment," Opt. Lett. **33**(22), 2626–2628 (2008).
20. L. V. Keldysh, "Ionization in field of a strong electromagnetic wave," Soviet Phys. JETP **20**(5), 1307 (1965).
21. H. S. Brandi and C. B. Dearaujo, "Multiphoton absorption-coefficients in solids – a universal curve," J. Phys. C Solid State Phys. **16**(30), 5929–5936 (1983).
22. M. Balu, L. Padilha, D. Hagan, E. Van Stryland, S. Yao, K. Belfield, S. Zheng, S. Barlow, and S. Marder, "Broadband Z-scan characterization using a high-spectral-irradiance, high-quality supercontinuum: erratum," J. Opt. Soc. Am. B **26**(8), 1663–1663 (2009).
23. R. A. Negres, J. M. Hales, D. J. Hagan, and E. W. Van Stryland, "Experiment and analysis of two-photon absorption spectroscopy using a white-light continuum probe," IEEE J. Quantum Electron. **38**(9), 1205–1216 (2002).
24. M. Balu, L. A. Padilha, D. J. Hagan, E. W. Van Stryland, S. Yao, K. Belfield, S. Zheng, S. Barlow, and S. Marder, "Broadband Z-scan characterization using a high-spectral-irradiance, high-quality supercontinuum," J. Opt. Soc. Am. B **25**(2), 159–165 (2008).
25. M. Sheik-Bahae, A. A. Said, T. H. Wei, D. J. Hagan, and E. W. Van Stryland, "Sensitive measurement of optical nonlinearities using a single beam," IEEE J. Quantum Electron. **26**(4), 760–769 (1990).
26. K. Ikeda and Y. Fainman, "Material and structural criteria for ultra-fast Kerr nonlinear switching in optical resonant cavities," Solid-State Electron. **51**(10), 1376–1380 (2007).
27. C. N. Ironside, "2-Photon Gain Semiconductor Amplifier," IEEE J. Quantum Electron. **28**(4), 842–847 (1992).

1. Introduction

The two-photon absorption (2PA) processes in semiconductors have been extensively studied both experimentally and theoretically, resulting in what are now well-established scaling rules that can accurately predict the degenerate two-photon absorption (D-2PA) of direct-gap semiconductors [1-3]. These scaling rules show that D-2PA is inversely proportional to the cube of the energy gap, E_g. This means that the D-2PA coefficients in narrow-gap semiconductors are two to three orders of magnitude greater than the absorption than in large-gap semiconductors. For example, ZnO (E_g = 3.2eV) has a D-2PA two-photon absorption coefficient, $\alpha_2 \approx 5$ cm/GW at 532 nm [4], while for InSb (E_g = 0.23eV), $\alpha_2 \approx 2$ cm/MW in the range 8 to 12 μm [5]. 2PA coefficients in the cm/MW range may prove useful for practical applications, but these scaling rules imply that such large values are not accessible in the near infrared (NIR)/visible (VIS) range. For non-degenerate two-photon absorption (ND-2PA), the energies of individual photons may approach intermediate-state resonances that allow the 2PA to become much larger than in the degenerate case. As is well known, in the case of 2PA for a two-band model, the dominant transitions are either inter-band ("direct/allowed") or intra-band "self/forbidden" [6]. This suggests that such intermediate state resonances can become significant only when using photons with energies either very small or approaching the bandgap energy, such that the two photons employed in the process would have extremely different energies. We recently presented results of extremely ND-2PA (END-2PA) in ZnSe and GaAs and its application to gated infrared detection using a GaN-based detector [7]. In this current work, we report on more extensive studies including several other semiconductors along with theoretical calculations showing that END-2PA can exceed their degenerate counterparts by two to three orders of magnitude. We consider END-2PA as a non-degenerate process where the possible "intermediate" states lie energetically very close to both the initial state (in the valence band) or the final state (in the conduction band). This generally implies that the lower energy photon is much less than half the bandgap, placing it in the mid-infrared (MIR) when the semiconductors have visible or NIR bandgaps. As the lower energy photon

#153971 - $15.00 USD Received 6 Sep 2011; revised 24 Oct 2011; accepted 25 Oct 2011; published 28 Oct 2011

moves further into the IR significant enhancements will be realized, but, may be influenced by thermal broadening of the Urbach tail due to electron/exciton phonon interaction [8,9]. This allows the extremely large 2PA coefficients, previously only seen in narrow-gap semiconductors, to be observed in larger-gap semiconductors such as CdTe, GaAs, ZnSe, ZnO, and ZnS. The large enhancement of 2PA can be useful for optical switching, infrared (IR) detection [10] and could have important consequences for lasers and amplifiers based on two-photon gain [11]. Making use of our previous work using Kramers-Kronig relations to obtain the dispersion of the nonlinear refraction [3,12], we also predict an enhancement of the non-degenerate nonlinear refractive index n_2; however, positive and negative contributions from the two-photon, Raman and AC-Stark terms lead to a smaller enhancement but an extremely rapid dispersion in the 2PA region.

2. Theoretical background

While data for ND-2PA exist from the earliest experimental papers [13], besides our recent results [6], no other data exist to our knowledge with a ratio of photon energies larger than 3.3 [14]. As seen from Eq. (1) this is an interesting realm to investigate since as the intermediate state for the transition approaches an eigenstate of the system, the 2PA is expected to diverge (of course adding in decay insures overall convergence). In the case of END-2PA there are two resonances that can be exploited. As predicted by Wherrett [6] and verified in Ref [4], the allowed-forbidden transitions dominate 2PA in direct-gap semiconductors so that the small energy photon can become near resonant to the "forbidden" or self-transition while the large energy photon can be nearly bandgap resonant. This is illustrated in Fig. 1, and may be easily seen qualitatively from the expression for the ND-2PA rate, W_2^{ND}, which can be written in the perturbative framework [15] as

$$W_2^{ND} = \frac{2\pi}{\hbar}\sum_{vc}\left|\sum_i\left[\frac{\langle c|H_2|i\rangle\langle i|H_1|v\rangle}{E_{iv}(\mathbf{k})-\hbar\omega_1}+\frac{\langle c|H_1|i\rangle\langle i|H_2|v\rangle}{E_{iv}(\mathbf{k})-\hbar\omega_2}\right]\right|^2\delta\left[E_{cv}(\mathbf{k})-\hbar\omega_1-\hbar\omega_2\right] \quad (1)$$

with indices *1* and *2* designating the two photons, *H* the electron-field interaction Hamiltonian and *v*, *c* and *i* the valence, conduction and intermediate states, respectively.

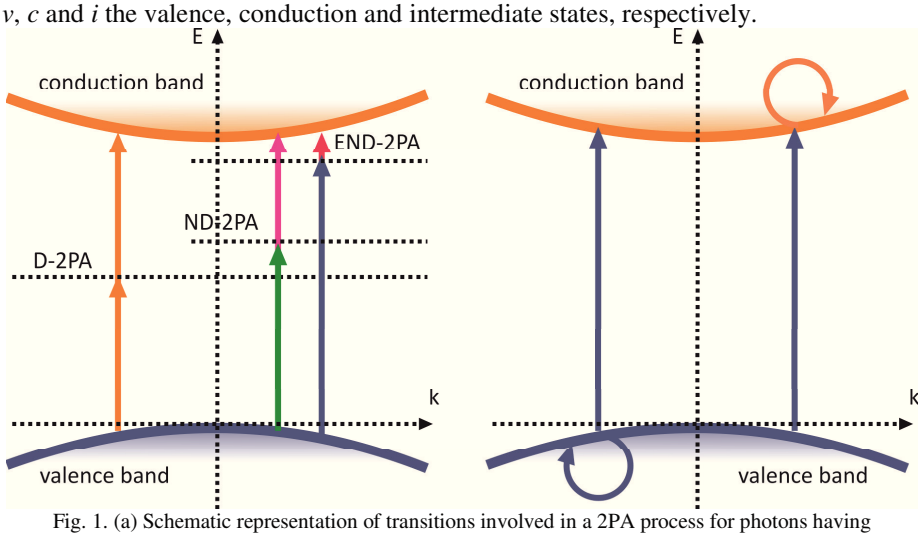

Fig. 1. (a) Schematic representation of transitions involved in a 2PA process for photons having various energy ratios, with ND-2PA and END-2PA characterized by a small detuning energy as compared to the bandgap. (b) The equivalent representation within the perturbative framework showing the possible transitions for two-band structure consisting of direct ("allowed") and self ("forbidden") transitions.

#153971 - $15.00 USD Received 6 Sep 2011; revised 24 Oct 2011; accepted 25 Oct 2011; published 28 Oct 2011

If one considers the simple model of a two-band direct-gap semiconductor, the virtual state can be taken as either the initial (in the valence band) or the final state (in the conduction band) for the electron transition, in which case one resonance occurs for both the low and high-energy photons (see Fig. 1b). For this case, since E_{iv} is either equal to 0 or to $E_{cv} = \hbar\omega_1 + \hbar\omega_2$, one can write explicitly the contributions from different paths of evolution for the system and obtain

$$W_2^{ND} \sim \left| \frac{M_{vc}^2 M_{vv}^1}{-\hbar\omega_1} + \frac{M_{vc}^1 M_{vv}^2}{-\hbar\omega_2} + \frac{M_{cc}^2 M_{vc}^1}{\hbar\omega_2} + \frac{M_{cc}^1 M_{vc}^2}{\hbar\omega_1} \right|^2, \tag{2}$$

where $M_{ij}^{1,2} = \langle j | H_{1,2} | i \rangle$ are the corresponding matrix elements. The matrix elements are linear in the amplitude of the magnetic vector potential associated with the respective fields, which in turn are expressed in terms of ratios of square root of irradiances divided by photon energies. Overall, taking also into account the expression of non-degenerate 2PA $\alpha_2(\omega_1;\omega_2) = \hbar\omega_1 W_2^{ND} / (I_1 I_2)$, we obtain a complex and stronger dependence on the photon energies of the interacting fields as exemplified below with the functional form of 2PA as derived in Ref [3]. Smaller photon energies will decrease the denominator values thus increasing the 2PA. It is important to observe here that each of the two different possible transition sequences yields a term enhanced significantly by the presence of a small energy photon. This effect is similar to the intermediate state resonance enhancement (ISRE) predicted and seen in molecular systems [14,16]. In direct-gap semiconductors the one-photon absorption (1PA) edges are generally sharper than those of organics and therefore larger enhancements may be obtained when probing very close to the linear absorption range.

Theoretical calculations of third-order nonlinearities in semiconductors are very well documented, and there are a couple of approaches commonly used in the past. One of the methods involves the use of second-order perturbation theory, as in Eq. (1), to directly calculate the transition rates using a quantum mechanical description (eigenvalues and eigenstates) of the considered systems. Reasonable predictions can be made either using a simple two-parabolic band model [6,17] or one can employ complex 4- or 7-band calculations for better accuracy, which can go as far as predicting the anisotropy of the nonlinear coefficients for particular systems like the ones exhibiting zinc-blende symmetry [15,18]. The 2PA spectra obtained with these models are similar as more complex numerical calculations only lead to shifts in the magnitudes of the coefficients producing minor changes to the spectral shapes [15]. This is quite different from the case of three-photon absorption (3PA) where different pathways result in quantum interference leading to very different results depending on the band model used [19]. Another theoretical method that was successfully used in the past and in the calculations shown in this paper, is based on Keldysh's tunneling theory [20]. It uses a scattering matrix formalism with Volkov-type "dressed" wavefunctions for the electronic states in order to account for the effect of the electric field on the system [3,17,21]. This provides similar 2PA spectra to the perturbation methods and yields identical results for the simple case of two-parabolic bands and D-2PA. As shown in Ref [3], the ND-2PA coefficient $\alpha_2(\omega_1;\omega_2)$ is calculated in this scattering matrix formalism with two parabolic bands to be:

$$\alpha_2(\omega_1;\omega_2) = K \frac{\sqrt{E_p}}{n_1 n_2 E_g^{\,3}} F_2\left(\frac{\hbar\omega_1}{E_g};\frac{\hbar\omega_2}{E_g}\right),$$
$$where \quad F_2(x_1;x_2) = \frac{(x_1 + x_2 - 1)^{3/2}}{2^7 x_1 x_2^2}\left(\frac{1}{x_1} + \frac{1}{x_2}\right)^2, \tag{3}$$

#153971 - $15.00 USD Received 6 Sep 2011; revised 24 Oct 2011; accepted 25 Oct 2011; published 28 Oct 2011

for the optical frequencies $\omega_{1,2}$, E_p is the Kane energy parameter, E_g is the bandgap energy, $n_{1,2}$ *are* the refractive indices, and K is a material independent parameter. We should mention here that a similar expression is obtained using the perturbation approach as shown in [15] (see Eqs. (15) and 16).

3. Experimental results

The experimental ND-2PA spectra presented in this paper are taken in a standard pump-probe non-collinear geometry with a small angle (~7 degrees) between the pump and the probe beams, using either picosecond or femtosecond pulses. The temporal scans are obtained by delaying either the pump (femtosecond data) or the probe (picosecond data) using a retroreflector mounted on a computer-controlled motorized translation stage. The picosecond pump-probe experiments are performed using a 10Hz EKSPLA laser system (PL-2143C). It consists of a ~30 ps FWHM modelocked Nd:YAG 1064 nm laser, converted to the third harmonic at 355 nm and pumping two LBO-based optical parametric generation/amplification (OPG/OPA) devices. The IR pump beam for our experiments is obtained through a difference frequency generation (DFG) process in a GaSe crystal using 1064 nm from the laser and the idler beam from a second similar OPG/OPA system. The IR pumping wavelength is chosen to be 8840 nm corresponding to approximately 10% of the bandgap of GaAs, which together with CdTe are the two semiconductors studied in this configuration. Our choice of pump wavelength is also based on the available tuning range of the IR (8-14 μm) and taking into account the energy and beam quality at the output wavelengths. The probe beam is selected by tuning the idler output to individual wavelengths in the near-IR. Our probe beam has a maximum energy of a few nJs and a smaller spot size than that of the pump, as measured by knife-edge scans, with a ratio of 1:2. This assures an irradiance in the probe beam smaller by at least a factor of 100 than the pump beam irradiance. In our configuration, this causes minimal losses through D-2PA of the probe (< 0.5%, which is at our noise level).

A similar setup is used for our femtosecond experiments. The system consists of a 1 kHz Clark MXR Ti:Sapphire laser pumping two BBO- based TOPAS OPG/OPA systems from Light Conversion Inc. with an infrared beam obtained through DFG in a $AgGaS_2$ crystal, like in the case of the picoseconds system. The pump used for these experiments is in the wavelength range of 1200 nm to 5600 nm, corresponding to approximately 30% to 8% of the bandgap energy for the semiconductors studied (ZnSe, ZnS, ZnO). Depending on wavelength, it can be either the idler output of the TOPAS or obtained through DFG. Autocorrelation measurements of the pulsewidths yield values of ~140 fs FWHM. The probe is obtained from a white-light continuum (WLC) generated using the 1300 nm signal beam from the TOPAS into a 2 mm thick piece of CaF_2. Individual wavelengths are selected from the WLC using a set of interference filters with a spectral bandwidth of ~10 nm. The temporal width of the spectrally filtered pulses is between 140 fs and 160 fs as verified by autocorrelation experiments [22]. The pump to probe spot size ratio is ~7 to 1 giving a minimum ratio for the pump to probe irradiance of 20. Similar to the picoseconds experiments, the probe energy is small enough that any self-induced probe beam 2PA can be neglected.

In all our nondegenerate experiments, the pump or excitation beam (I_e), is always at the longer wavelength, with photon energies less than a third of the bandgap. This is to avoid any 2PA or 3PA caused by the pump itself which would complicate the experiment and the analysis of the experimental data, and would lead to the creation of free-carrier pairs which would cause extra losses especially for longer pulses. Hence, absorption is solely caused by ND-2PA with one photon being absorbed from each beam. Although this absorption also produces free carriers, the density of carriers produced is proportional to the photon density from the weak probe beam which is deliberately kept very small. For our experiments, effects of free-carrier absorption and refraction can be ignored altogether. Thus, the irradiance dependent pump-probe results are modeled by,

#153971 - $15.00 USD Received 6 Sep 2011; revised 24 Oct 2011; accepted 25 Oct 2011; published 28 Oct 2011

$$\frac{dI_p(\omega_p)}{dz} = -2\alpha_2(\omega_p;\omega_e)I_e(\omega_e)I_p(\omega_p). \quad (4)$$

The second reason the low photon energy beam is used as the pump is related to the magnitude of the 2PA coefficient, which scales with the photon energy at which the absorption is monitored. The frequency dependence of the 2PA coefficient (3) through the F_2 function leads to the relation $\alpha_2(\omega_p;\omega_e)/\alpha_2(\omega_e;\omega_p) = \omega_p/\omega_e$. This is because the rate of photon loss must be the same for both beams, hence the energy loss rate is larger for the beam with higher energy photons. Because the photon loss rates are identical, the carrier generation rate is symmetric in the two wavelengths. Thus, as noted in [7], the END enhancement in two-photon detection is the same regardless of which wavelength is the signal or the gate.

The use of a low frequency pump allows for the variation of the probe frequency only over a limited range set by the lowest energetically possible transition and the linear absorption edge, i.e. the probe photon energy can be varied between E_g - $\hbar\omega_e$ and E_g. Typical experimental data are shown in Fig. 2 for CdTe with picosecond pulses (a) and ZnO with femtosecond pulses (b). In the picosecond experiments, $\hbar\omega_e$ is approximately 9.3% of the CdTe bandgap. For the case of femtosecond experiments there are more choices for the pump wavelength. In ZnO, for instance, we are able to choose $\hbar\omega_e$ equal to ~32%, 23%, 19.5%, 17% and 15.5% of E_g. The lowest pump energy corresponds to 2.5 μm which is at the end of our femtosecond OPG/OPA tuning range. Using DFG we also used a pump wavelength of 5.6 μm in ZnSe, which corresponds to about 8% of the bandgap energy.

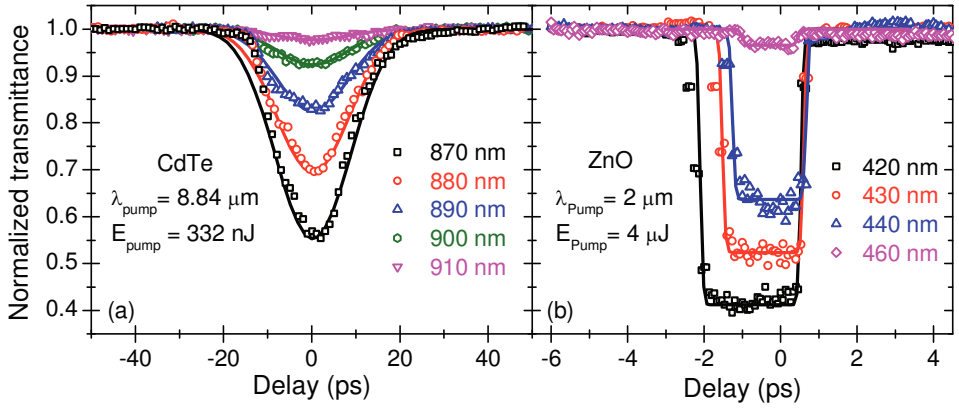

Fig. 2. Typical experimental pump-probe data in CdTe (a) using picoseconds pulses and ZnO (b) using femtosecond pulses along with theoretical fits (solid lines).

For femtosecond pulses, group velocity dispersion (GVD) plays a very important role. This is apparent in the shape of our temporal pump-probe curves as seen in Fig. 2b. Because the group velocity varies strongly with wavelength, for a large range of initial delays, the pump (fast) and probe (slow) walk through each other as they propagate through the sample. The measured effect is a consequence of "effective" temporal overlaps, and as this "effective" overlap distance is smaller than the sample thickness we obtain the same change in transmittance for a range of initial delays. The data were analyzed taking these effects into consideration according to the treatment given in [23]. It should be mentioned that the new femtosecond data shown here is collected without the use of modulation techniques unlike in our previous publication [7].

In Fig. 3 (a) we show the measured END-2PA spectra of GaAs and CdTe along with the calculated curves and plotted versus the average photon energy, thus comparing the coefficients for two transition processes between the same energy levels. This allows convenient representation of the data on the same graph along with the degenerate 2PA

#153971 - $15.00 USD Received 6 Sep 2011; revised 24 Oct 2011; accepted 25 Oct 2011; published 28 Oct 2011

spectrum taken with the femtosecond system using the Z-Scan technique [24]. In all our plots the photon energies are shown scaled to the respective bandgap energies since this allows comparing different semiconductors on the same scale and makes the comparison to the respective degenerate values easier. The theoretical values are represented with solid lines together with measured degenerate data. The measured nondegenerate values are as large as 1 cm/MW, ~180 × larger than the corresponding degenerate values and about 40 × larger than the peak value for the degenerate 2PA. There is a remarkable agreement between the measured and the predicted values using the simple two parabolic-band model over a large range of photon energies. This agreement is not entirely surprising since in experiments with very nondegenerate photons the states involved in transitions are close to the center of the Brillouin zone where the parabolic approximation works best. However, we are able to measure some small signals when the sum of the energies of the two photons falls below the band edge. The analysis shows that the signals are linear in pump energy confirming a ND-2PA process as we are accessing states within the Urbach tail. Due to the large enhancement we are able to measure such small contributions which would otherwise be impossible to do using degenerate photons. Thus END-2PA may be useful for studying the impurity and defect absorption in the Urbach tail.

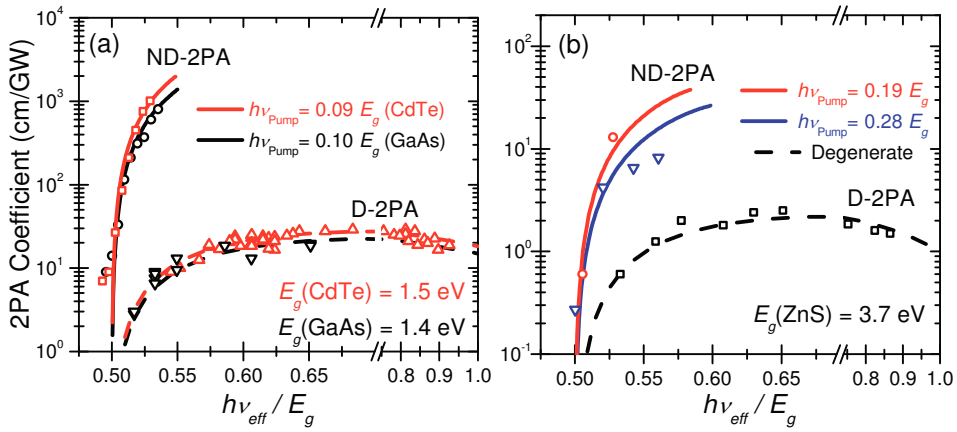

Fig. 3. Non-degenerate 2PA spectra of CdTe and GaAs measured with picosecond pulses (a) and of ZnS measured with femtosecond pulses (b). The theoretically calculated non-degenerate spectra are shown with straight lines, while the dashed lines denote the respective degenerate spectra, along with measured degenerate data. The non-degenerate data in GaAs was taken from [7].

A summary of results obtained using femtosecond pulses is presented in Fig. 3(b) for ZnS and in Fig. 4 for ZnSe (a) and ZnO (b). For these cases the choices of pump and probe photon energies are limited by the specifics of our experimental apparatus. Taking data with small photon energies in the pump beam proved difficult for the largest bandgap semiconductors, since for these cases the probe photons are close to the UV, and in our continuum the energies available for this part of the spectrum are low. The smallest pump photon energy corresponds to approximately 15.5%, 8% and 19% of the bandgap of ZnO, ZnSe and ZnS, respectively. Consequently, the measured maximum enhancement of the nondegenerate values with respect to the degenerate ones varies strongly with the pump photons' energy, reaching ~40 in ZnO and ~270 in ZnSe. As shown, there is again good agreement between theory and femtosecond experimental data. Similarly, the plotted degenerate data was taken using the femtosecond system using the Z-scan technique [25].

#153971 - $15.00 USD Received 6 Sep 2011; revised 24 Oct 2011; accepted 25 Oct 2011; published 28 Oct 2011

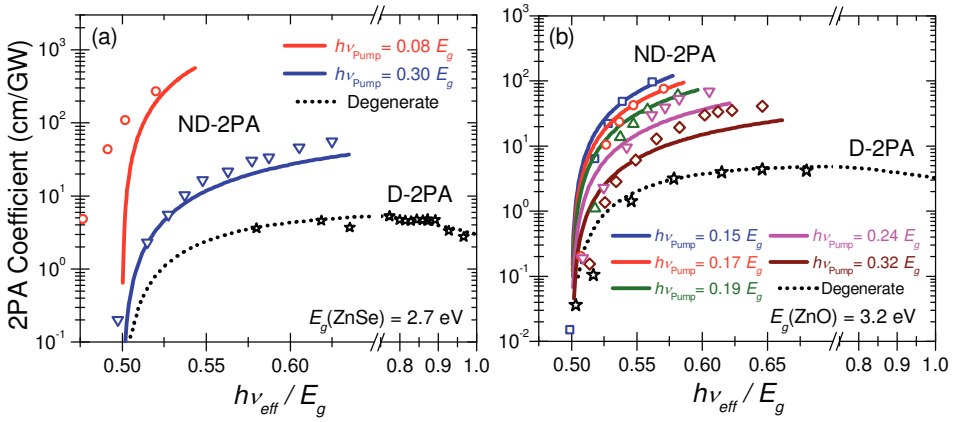

Fig. 4. Non-degenerate 2PA spectra of ZnSe (a) and ZnO (b) measured with femtosecond pulses. The theoretically calculated non-degenerate spectra are shown with straight lines, while the dashed lines denote the respective degenerate spectra, along with measured degenerate data. The 2PA data in (a) was taken from [7] and the degenerate data in (b) was taken from [24].

4. Discussion

The data taken on ZnO best illustrates the strong dependence of the measured values on the pump wavelength. The longer the pump wavelength, the stronger is the enhancement seen in the 2PA. The largest overall magnitude we measure is about 1 cm/MW using the mid-IR pump. We point out here that these nonlinearities are measured at visible and near IR wavelengths and their magnitudes come close to the degenerate values measured in narrow-gap semiconductors (e.g. InSb, InAs, etc.) at wavelengths in the mid-infrared. This can be understood by considering the perturbative expression (Eq. (2) of the 2PA rate when using a simple two-band model for a given pair of initial and final states. For the nondegenerate case, the energy term in the denominator gets as small as the pump energy with one of the two terms being highly enhanced for either of the transition paths possible (a first "self" transition followed by a direct transition or vice versa) as is written in Eq. (5) .

$$W_2^{\,D} \propto \left| \frac{M_{vc}^{(2)} M_{vv}^{(2)}}{-\hbar\omega_2} + \frac{M_{cc}^{(2)} M_{vc}^{(2)}}{\hbar\omega_2} \right|^2 . \qquad (5)$$

If we now consider the case of D-2PA in a direct narrow-gap semiconductor at the pump wavelength (energy of $\hbar\omega_2$), we obtain two terms with the same denominator energy values. Since the momentum matrix elements depend mainly on the symmetry of the bands involved [13], for similar systems (zincblende structures for instance) we should expect values of the same order of magnitude. The difference here, however, is the necessity of having only one long wavelength photon. Also, to obtain the highest nonlinearities it is necessary to probe close to the linear absorption edge, effectively narrowing the available spectral range. To overcome this, a very high quality sample should be used, possibly at a low temperature in order to minimize any linear losses on the probe beam. However, there is an upper limit to the nonlinearities that can be obtained in a nondegenerate configuration. The main limitation is the linear absorption at the probe wavelength below the bandgap, i.e. Urbach tail absorption. Assuming the upper energy limit for the probe photons set to 0.97 of the bandgap energy, by using pump photons at about 5% of the bandgap energy one would theoretically obtain an increase of the 2PA coefficient of only about 2 × versus pumping with photons at 10% of the bandgap. It is important to mention that such enhancements can be obtained in any direct-gap system provided that appropriate photon pairs are used. In systems with strict selection rules

#153971 - $15.00 USD Received 6 Sep 2011; revised 24 Oct 2011; accepted 25 Oct 2011; published 28 Oct 2011

there are additional restrictions which may put an upper practical limit on the measured enhancement [14].

For the highly nondegenerate experiments, the behavior of the Kerr index in particular spectral ranges is also very interesting. The nondegenerate nonlinear index can be obtained using the general expression of the change in absorption caused by the presence of a pump beam and performing a Kramers-Kronig transformation [3,9]. The nonlinear refractive index contains contributions from the 2PA, Raman and Stark processes.

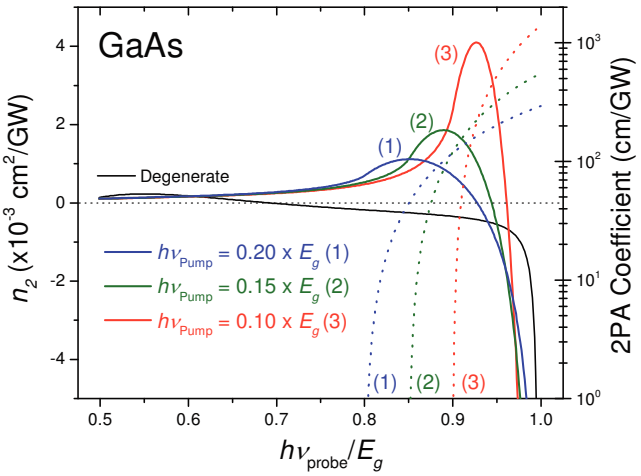

Fig. 5. Calculated nondegenerate induced refraction index (solid lines) and nondegenerate 2PA (dotted lines) of GaAs for pump energies equal to (1) 20% (4.32 μm), (2) 15% (5.81 μm) and (3) 10% (8.84 μm) of the bandgap.

As discussed explicitly in Ref [3], the 2PA terms gives the main contribution, positive for lower energy photons and negative for energies close to the bandgap. The Stark terms give an overall negative contribution to the nonlinear index, which increases asymptotically close to the band edge, while the Raman term adds positively.

For the nondegenerate case, this makes the calculated overall enhancement relatively smaller than for 2PA when using small photon energy pumps. The nonlinear index takes positive values (focusing nonlinearity) for small probe frequencies and turns negative (defocusing nonlinearity) for frequencies close to the 1PA edge. The probe frequency for which the nonlinear index becomes zero depends strongly on the pump frequency. This zero crossing occurs near the peak of the 2PA for the degenerate case approaching frequencies very close to the linear absorption edge as the energy of the pump photons is decreased. The slope of the spectrum near the zero crossing point also changes strongly with the pump photons' energy and becomes extremely steep for small energy pump photons. This leads to changes in the sign of the refractive nonlinearity over very narrow spectral ranges. These trends are shown in Fig. 5 for the particular case of GaAs.

When pumping at ~10% of the bandgap (8.84 μm), by varying the probe wavelength by ~13 nm, from 903 nm to 916 nm, we can vary the n_2 from -2×10^{-12} cm^2/W to 2×10^{-12} cm^2/W, numbers that in absolute value correspond to about 50% of the peak n_2. To verify this, picosecond pulses would be more suitable because of their narrower spectral widths; however, it would also be interesting to study the effect of this spectral dependence on a femtosecond pulse with a large bandwidth centered near the zero crossing frequency. Unfortunately, from the standpoint of applications, the nonlinear refraction is largely enhanced in spectral regions where the 2PA is also enhanced, see Fig. 5. To minimize losses, future applications would require avoiding these enhanced 2PA ranges, making use of only moderate enhancements in nonlinear refraction and the judicious choice of direct-gap semiconductor.

#153971 - $15.00 USD Received 6 Sep 2011; revised 24 Oct 2011; accepted 25 Oct 2011; published 28 Oct 2011

5. Conclusions

We measure nondegenerate 2PA spectra of several semiconductors (CdTe, GaAs, ZnS, ZnSe, and ZnO) using pairs of extremely nondegenerate photons. The magnitude of the 2PA coefficients increases dramatically when low energy pump photons, compared to the bandgap energy, are used. Very good agreement with calculations based on the "dressed" wavefunctions approach is shown. For our experiments in ZnSe, the measured non-degenerate 2PA is as large as 270 × the corresponding degenerate 2PA value when pumping with low energy photons of 0.08 E_g. This corresponds to a 50 × increase over the peak degenerate 2PA coefficient. Using even lower photon energies is theoretically predicted to lead to larger enhancements. The large nonlinearities measured, minimization of free-carrier effects, and the possibility to tailor the Kerr index behavior by the appropriate choice of wavelengths, suggest that efficient all-optical switching may be implemented [26]. These large enhancements made possible the demonstration of gated detection in a room temperature GaN photodiode with very good sensitivity [6]. This large enhancement of the 2PA coefficient also translates directly to enhanced two-photon gain [27], which opens the possibility of highly nondegenerate two-photon tunable laser and amplifier device applications [8]. However, it remains to be seen if the strong enhancement in two-photon emission would be sufficient to overcome the large free-carrier losses of the infrared wave in such devices.

Acknowledgements

This work was supported in part by the US Army Research Office (grant no. 50372-CHMUR) and the DARPA ZOE program (grant no. W31R4Q-09-1-0012).

#153971 - $15.00 USD Received 6 Sep 2011; revised 24 Oct 2011; accepted 25 Oct 2011; published 28 Oct 2011

PROV_DISC_2 1335P011

Extreme Nondegenerate Two-Photon Absorption in Semiconductors, END-2PA;

Eric Van Stryland, C. Cirloganu, D. Fishman, S. Webster, L. Padilha, D. Hagan

http://www.creol.ucf.edu

Summary

- Get orders of magnitude increase in 2PA with extreme nondegeneracy >10/1 in photon energy
  - ZnSe, CdTe, GaAs, ZnO, ZnS and GaN detector
- Use for detection of 390nm (below the gap) in GaN photodiode with 5.6 μm pump
- Use for detection of 5.6 μm in GaN photodiode with 390nm pump ~ as good as LN HgCdTe!
- Gated detection (sub-fs) of short pulses

Calculating 2PA in semiconductors

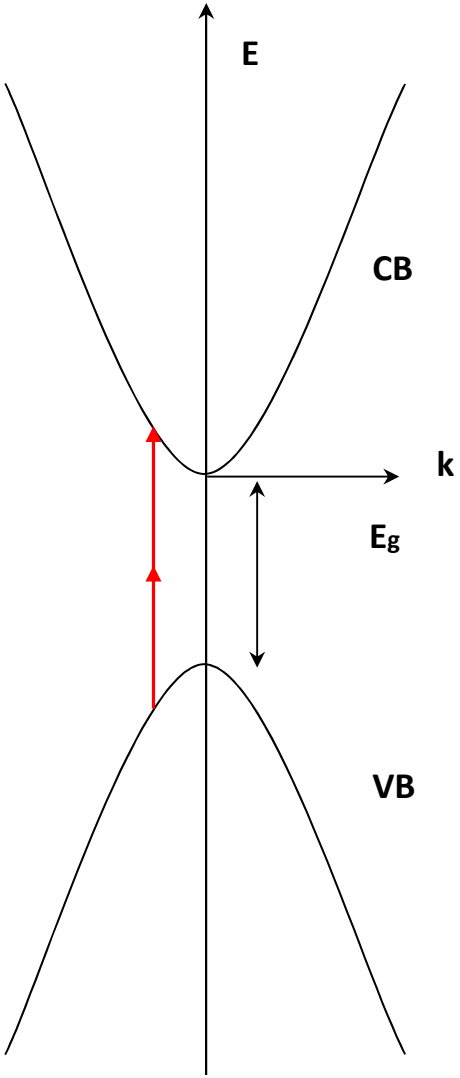

Perturbative approach

Allowed-forbidden transitions dominate

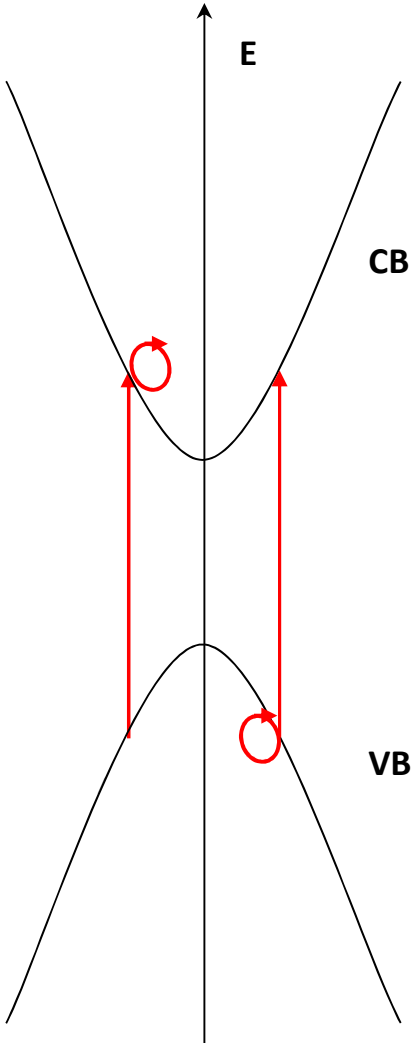

B.S. Wherrett, JOSA B **1**, 67 (1984)

2PA and scaling laws

Degenerate

$$\alpha_{2,th}(\omega) = K_2 \frac{\sqrt{E_p}}{n_0^2 E_g^3} \frac{(2\hbar\omega/E_g - 1)^{3/2}}{(2\hbar\omega/E_g)^5} \rightarrow F_2(\hbar\omega/E_g)$$

Degenerate

$$\alpha_{2,scaled} = \frac{\alpha_2(\omega) n_0^2}{K_2 \sqrt{E_p} F_2(x)} \propto \frac{1}{E_g^3}$$

Non-Degenerate

$$\alpha_2(\omega_1;\omega_2) = K \frac{\sqrt{E_p}}{n_1 n_2 E_g^{\ 3}} F_2\left(\frac{\hbar\omega_1}{E_g};\frac{\hbar\omega_2}{E_g}\right)$$

Non-Degenerate

$$F_2^{\ 2PA}(x_1;x_2) = \frac{(x_1 + x_2 - 1)^{3/2}}{2^7 x_1 x_2^{\ 2}} \left(\frac{1}{x_1} + \frac{1}{x_2}\right)^2$$

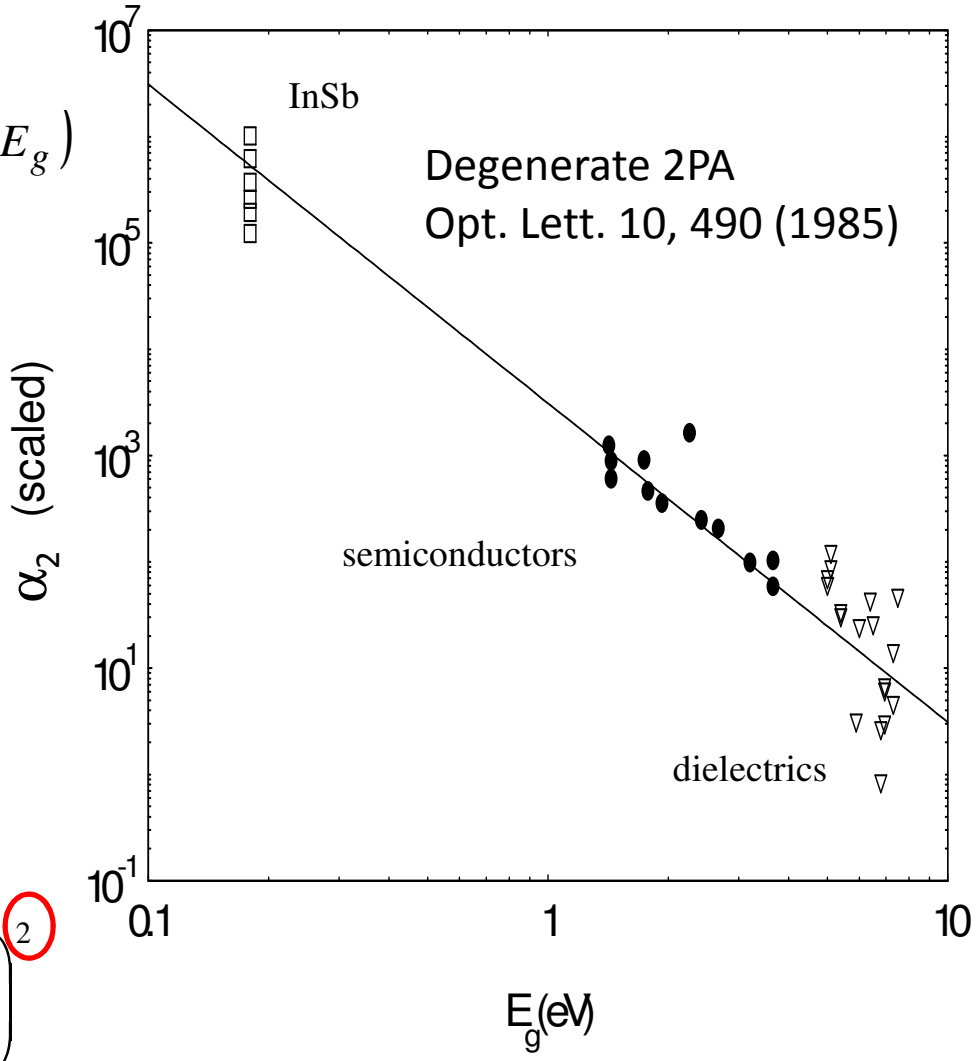

Phys. Rev. Lett., 65, 96-99 (1989)

Perturbative approach (2-band model)

$$W_{2\omega_2}^{NDD} = \frac{2\pi}{\hbar} \sum_{v,c} \left| \sum_i \left[\frac{M_{vc}^{2} M_{iv}^{1} H_{2}}{\hbar\omega_1 E_{iv}(\mathbf{k}) - \hbar\omega_2} + \frac{M_{ci}^{2} M_{vc}^{1} H_{1}}{\hbar E_{ic}(\mathbf{k}) - \hbar\omega_1} \right] \right|^2 \delta[E_{cv}(\mathbf{k}) - \hbar\omega_1 - \hbar\omega_2]$$

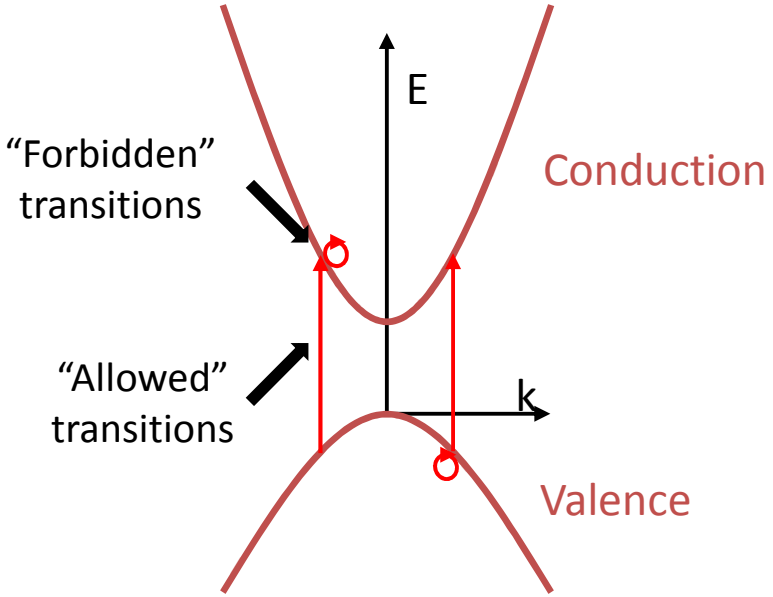

Highly enhanced!

$$\hbar\omega_2 = 0.1 E_{cv}$$

$$E_{cv} = \hbar\omega_1 + \hbar\omega_2$$

$$M_{ij}^{1,2} = \langle j | H_{1,2} | i \rangle$$

Perturbative approach (2-band model)

Large gap

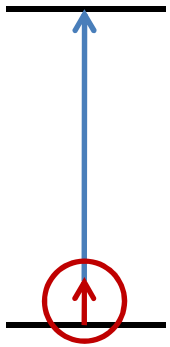

Narrow gap

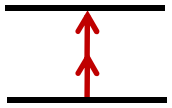

$$W_2^{ND} \propto \left| \frac{M_{vc}^{(2)} M_{vv}^{(1)}}{-\hbar\omega_1} + \frac{M_{vc}^{(1)} M_{vv}^{(2)}}{-\hbar\omega_2} + \frac{M_{cc}^{(2)} M_{vc}^{(1)}}{\hbar\omega_2} + \frac{M_{cc}^{(1)} M_{vc}^{(2)}}{\hbar\omega_1} \right|^2$$

$$W_2^{D} \propto \left| \frac{M_{vc}^{(2)} M_{vv}^{(2)}}{-\hbar\omega_2} + \frac{M_{cc}^{(2)} M_{vc}^{(2)}}{\hbar\omega_2} \right|^2$$

For similar structures we should have comparable magnitudes!

END-2PA: Enhancement Depends on Pump Frequency

ZnO

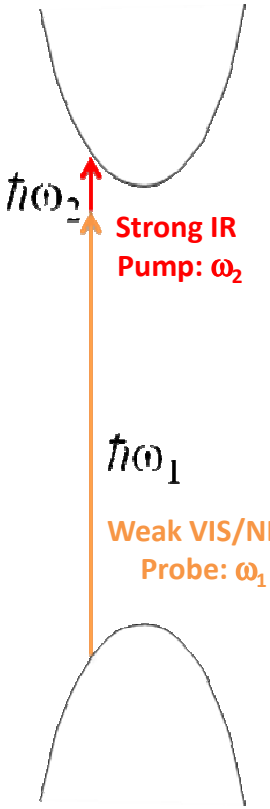

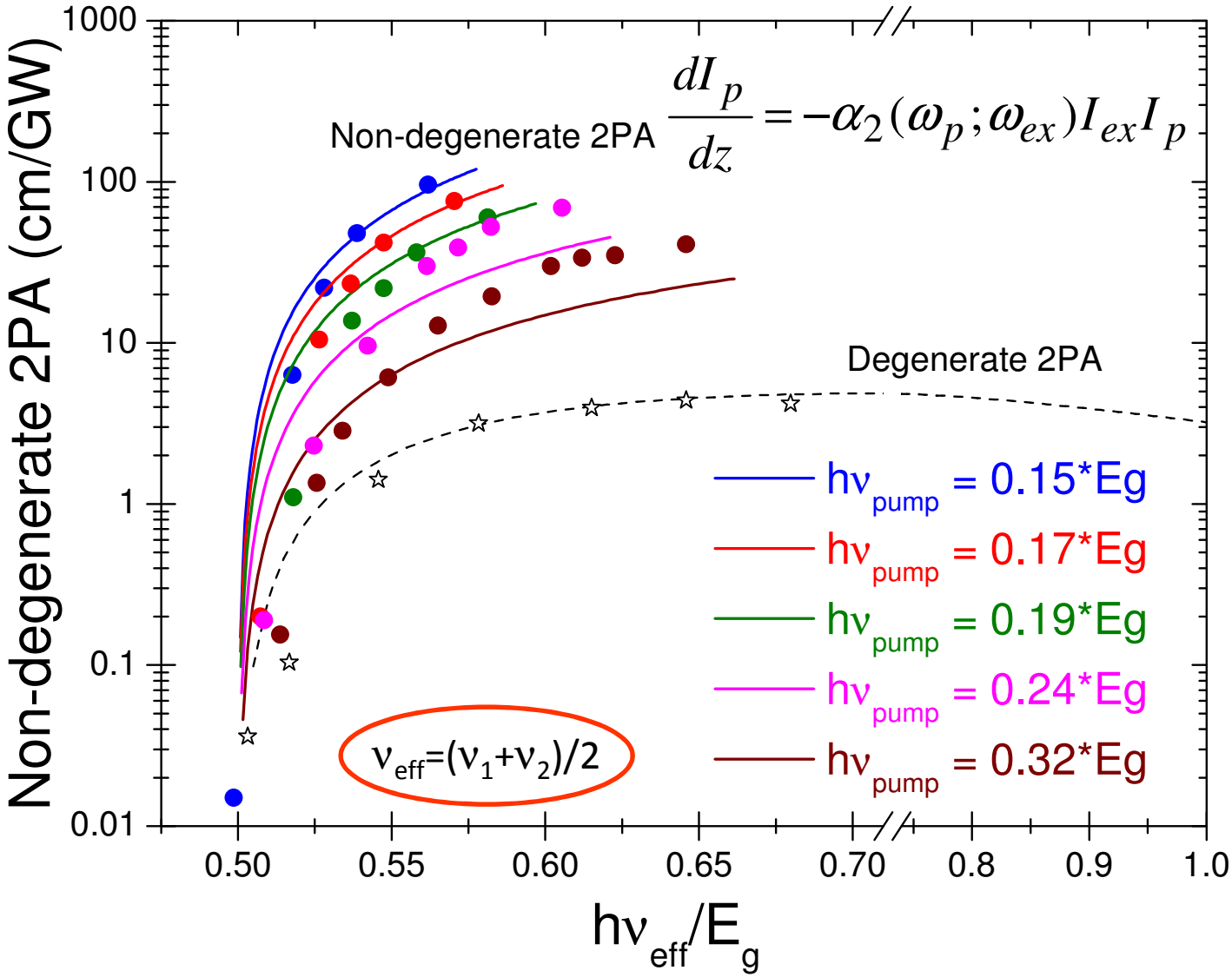

Pump-Probe

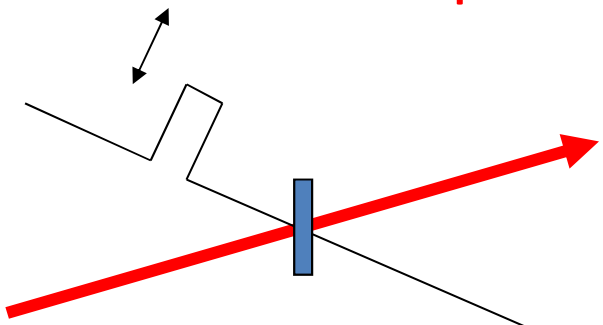

Pump/probe
with time delay

$$\frac{dI_p}{dz} = -\alpha_2(\omega_p;\omega_{ex})I_{ex}I_p$$

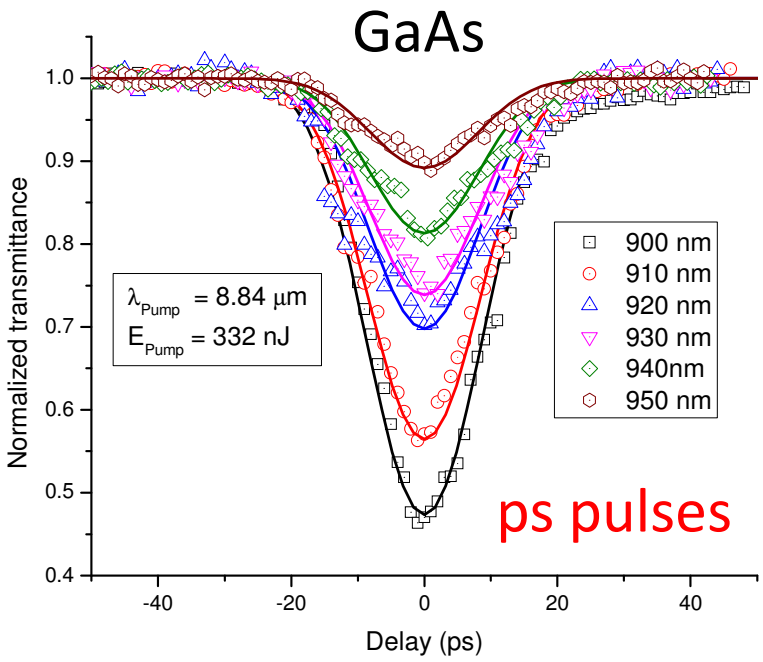

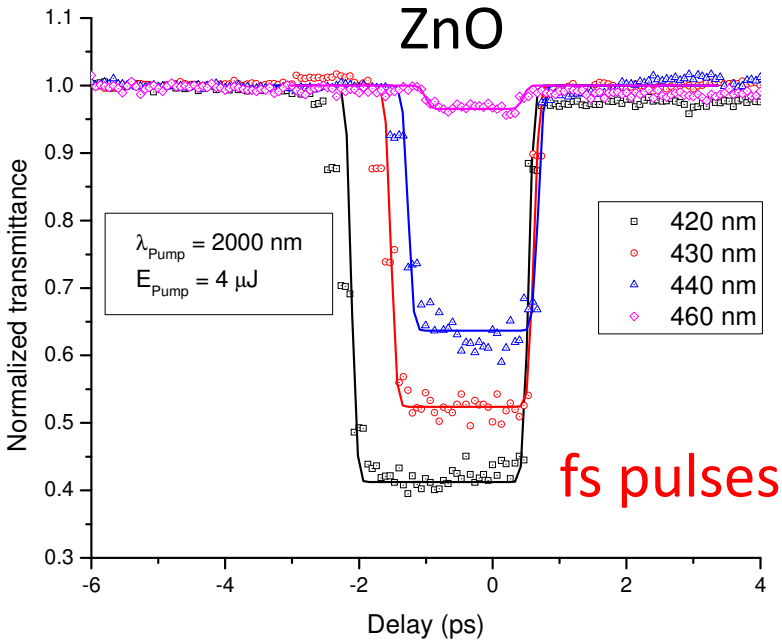

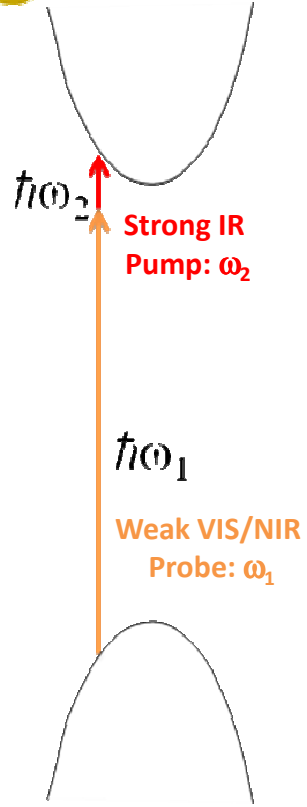

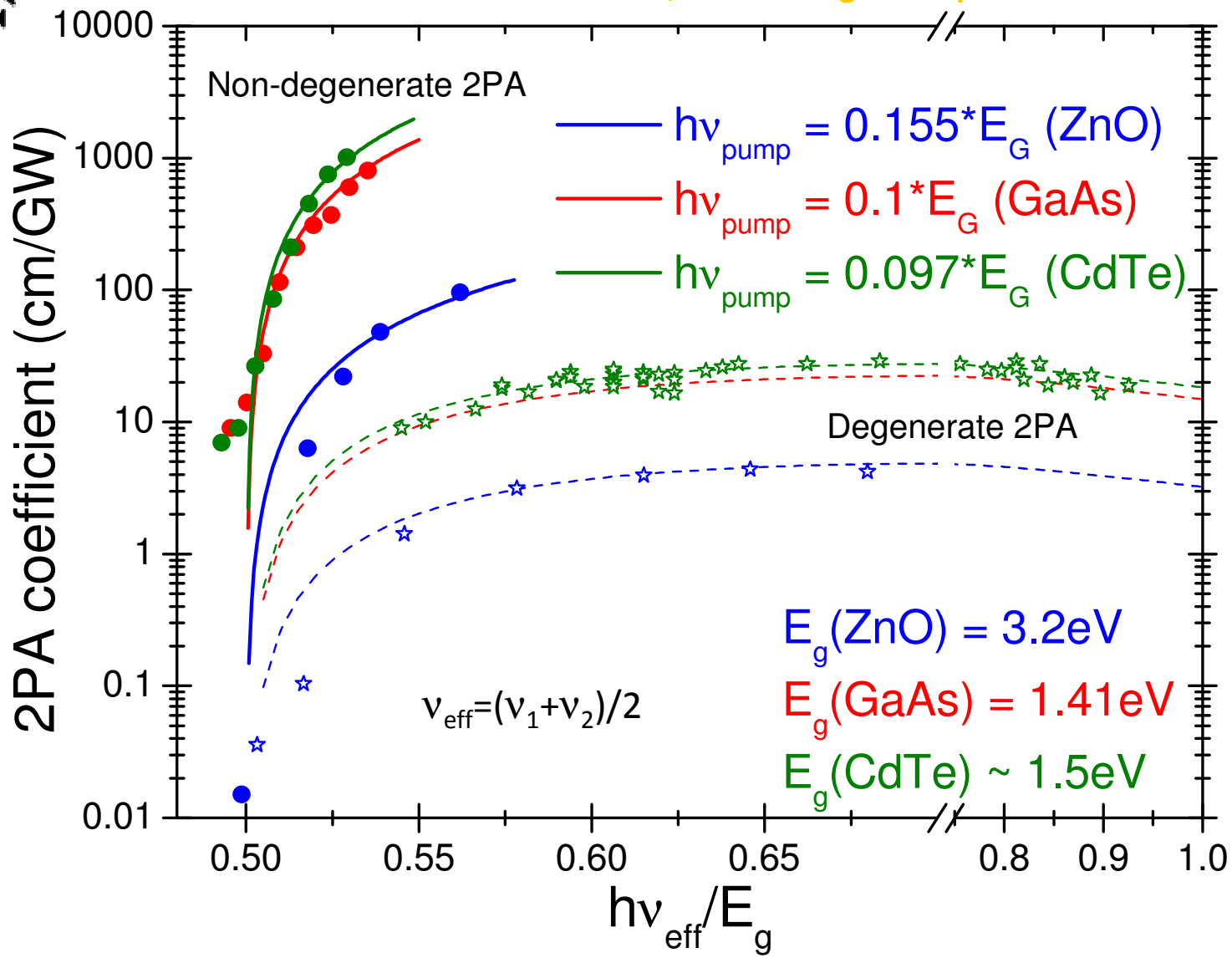

- **Maximum enhancement of 180 versus the corresponding degenerate value.**
- **Largest non-degenerate 2PA is 1 cm/MW**

ZnSe

E_g=2.67 eV

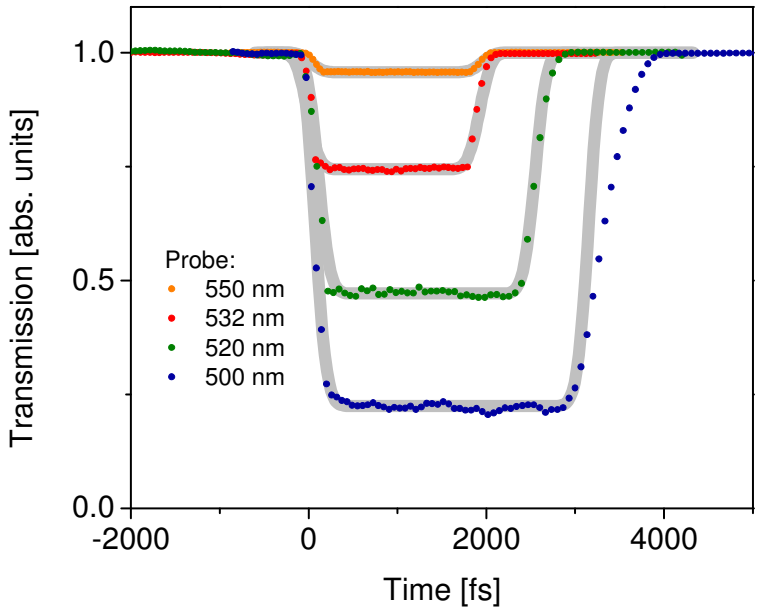

2PA signal vs time delay showing GVD

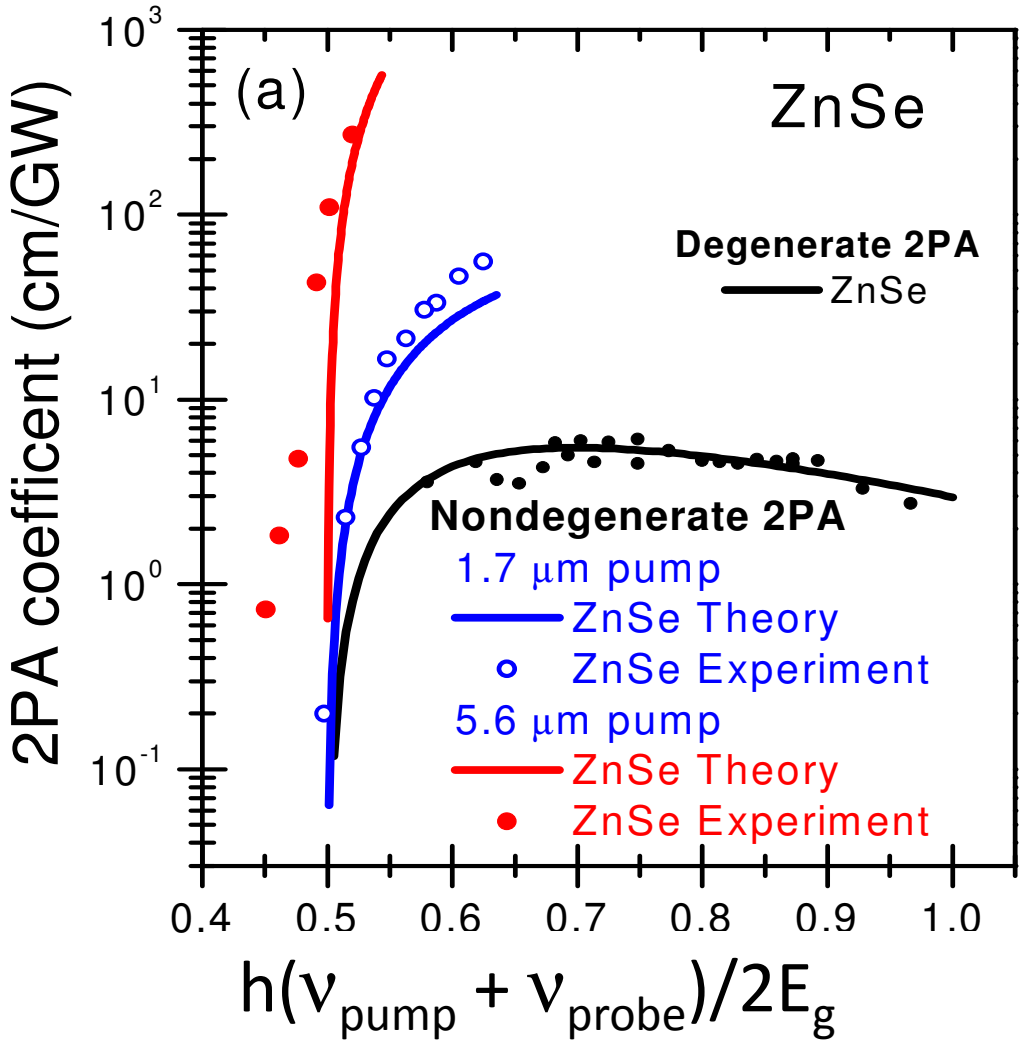

Extremely NonDegenerate 2PA

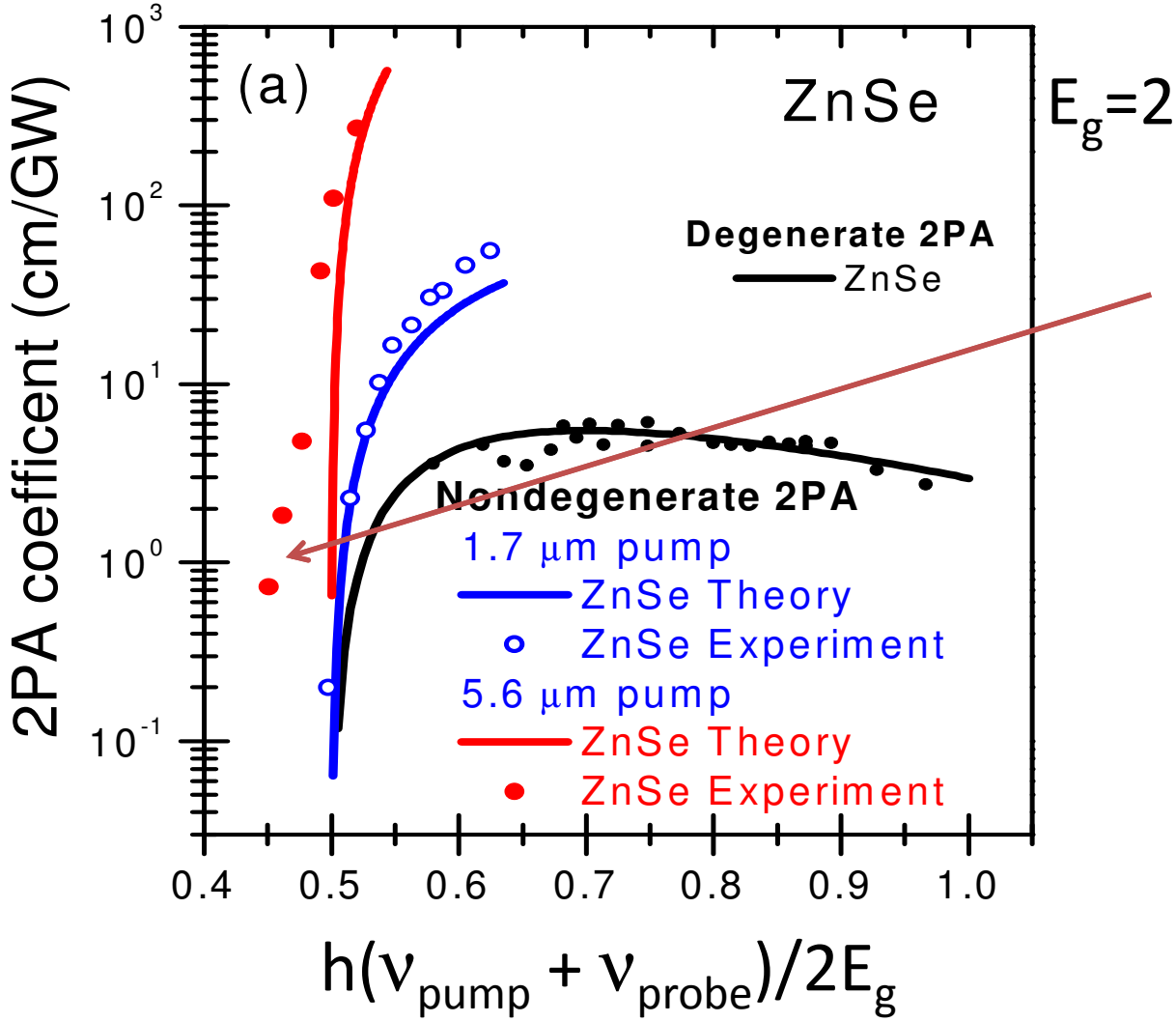

Urbach tail
Excitons
Impurities
Defects

Gated Detection in GaN E_g=3.28 eV

$$\frac{dI_p}{dz} = -\alpha_2(\omega_p;\omega_{ex})I_{ex}I_p$$

excite: 5.6 μm, 300 nJ
0.4GW/cm^2
probe: 390 nm

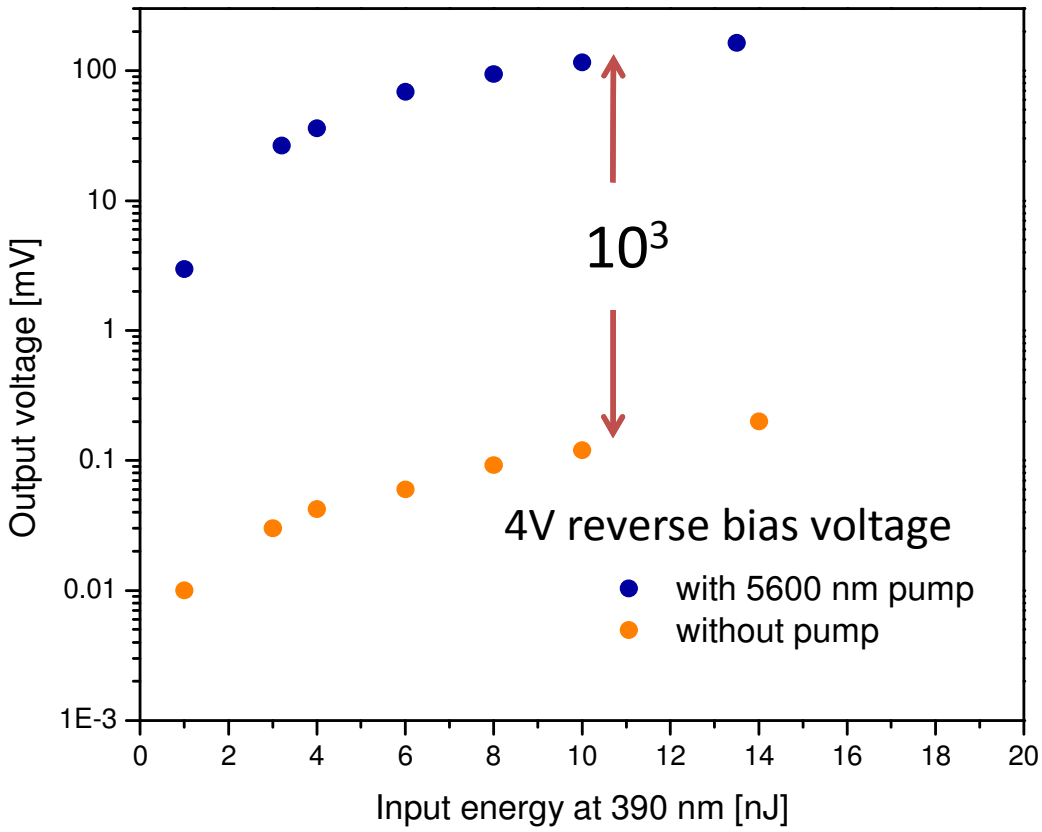

Cross correlation

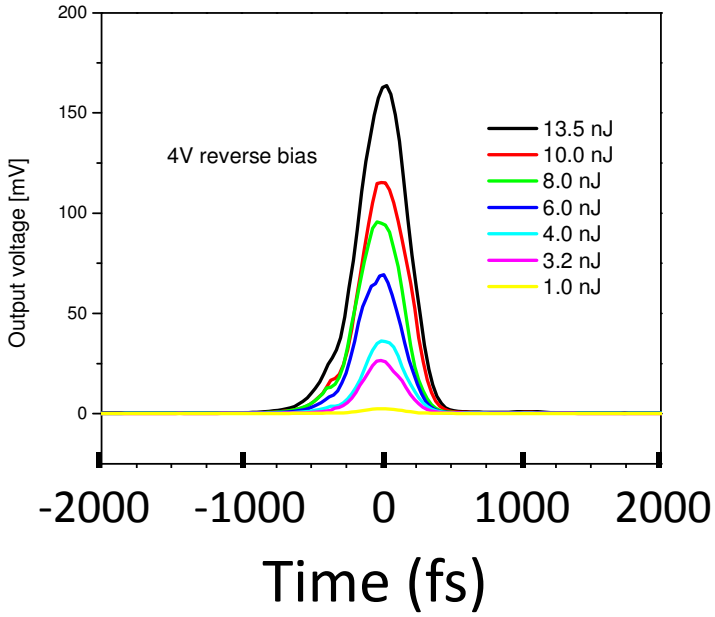

$$F_2^{2PA}(x_1;x_2) = \frac{(x_1+x_2-1)^{3/2}}{2^7 x_1 x_2^2}\left(\frac{1}{x_1}+\frac{1}{x_2}\right)^2$$

Note: pumping at long λ, probing at short λ

Detector response at 390 nm

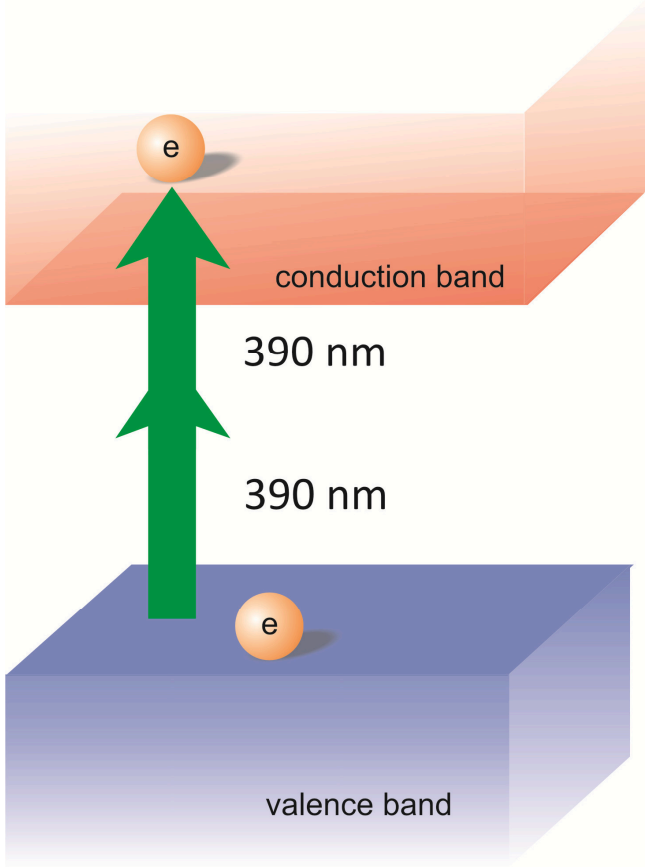

Quadratic dependence - Degenerate 2PA

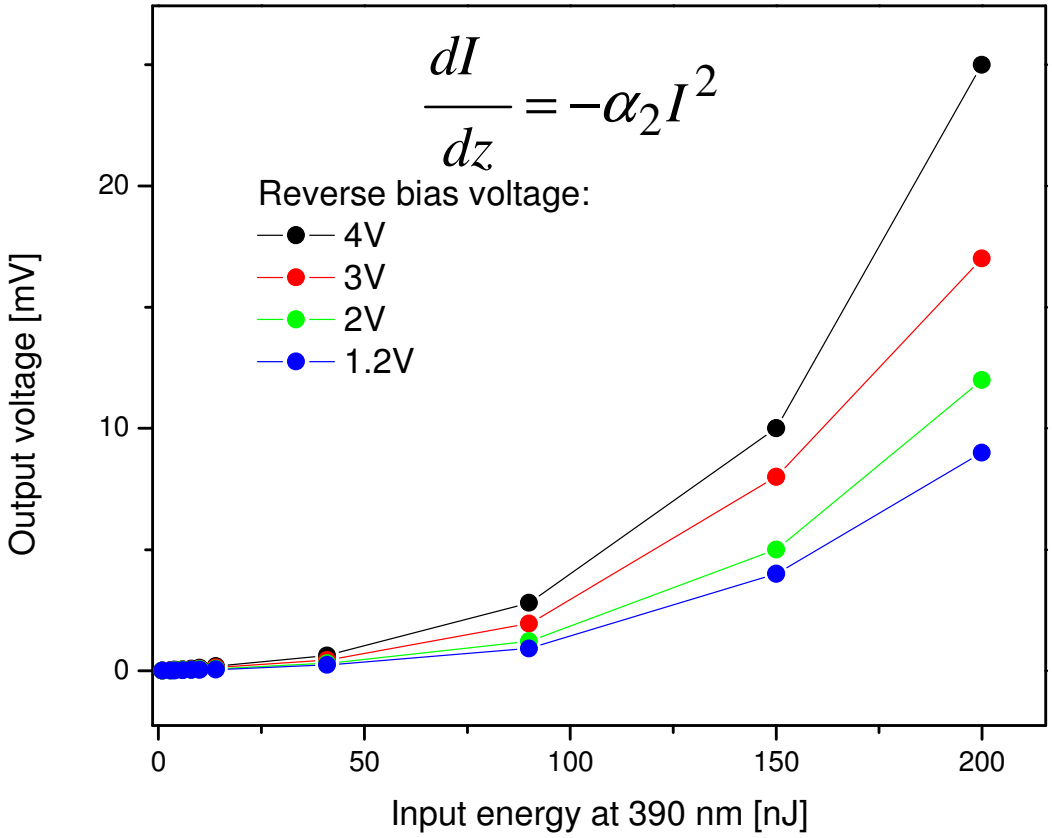

GaN detector response for different processes

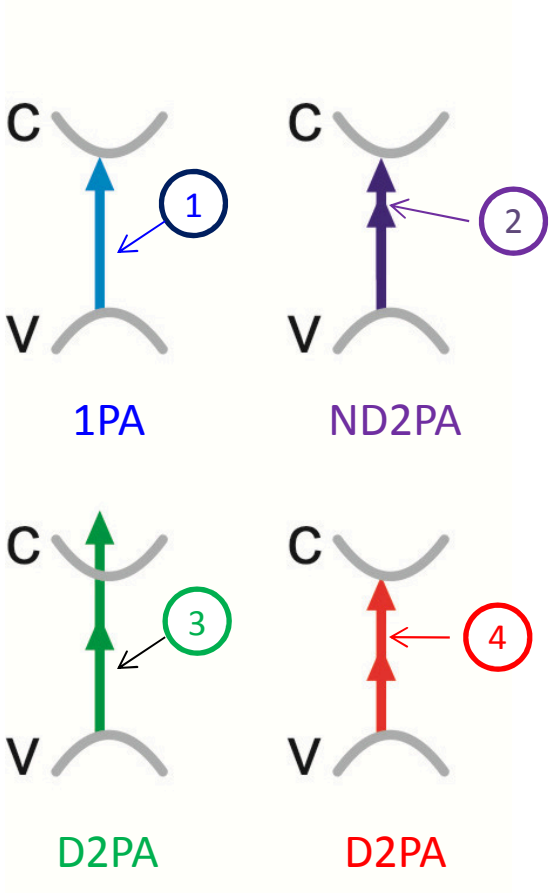

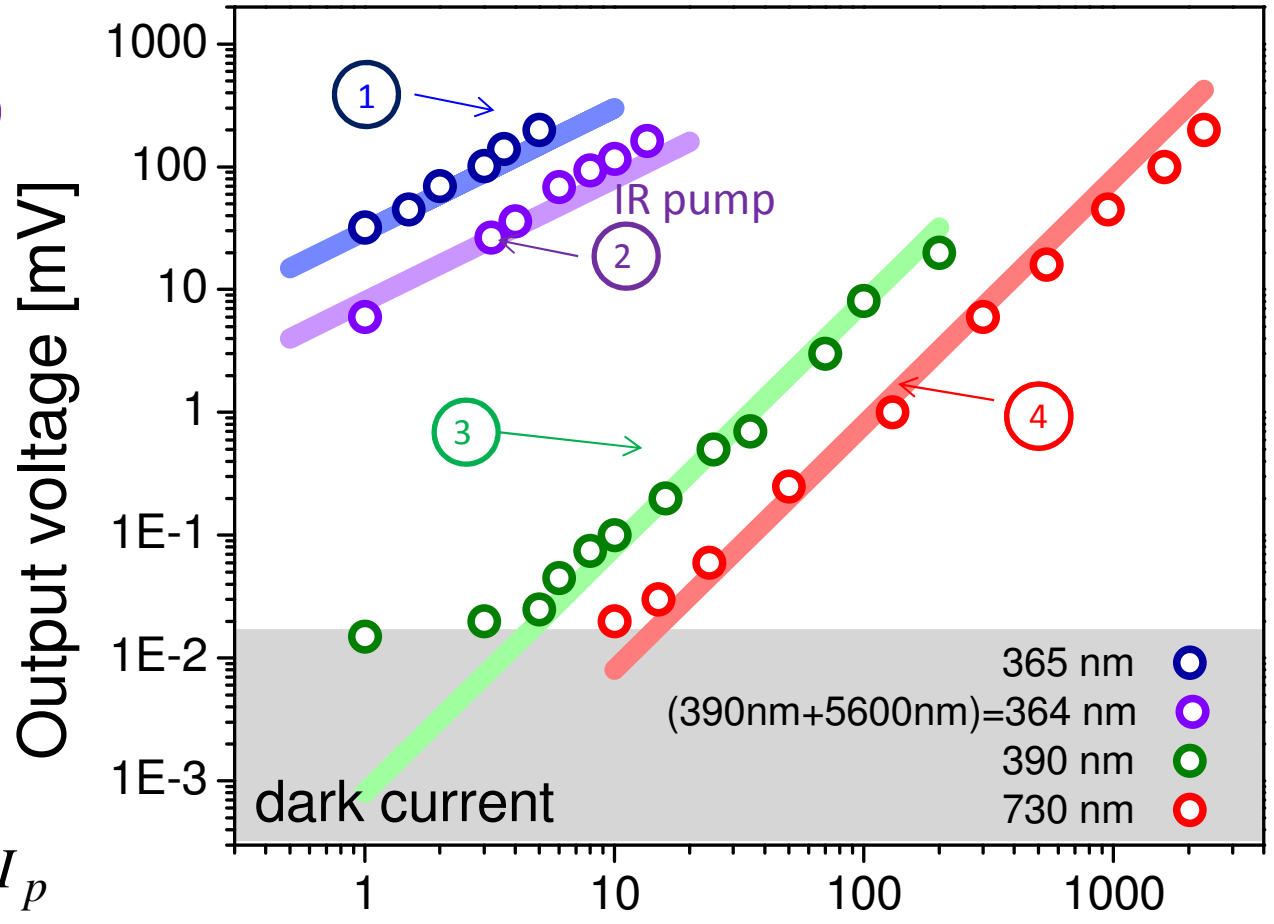

$$\frac{dI_p}{dz} = -\alpha_2(\omega_p;\omega_{ex})I_{ex}I_p \quad (2)$$

$$\frac{dI_{ex}}{dz} = -\alpha_2 I_{ex}^2 \quad (3)\ (4)$$

GaN detector response for different IR pump powers

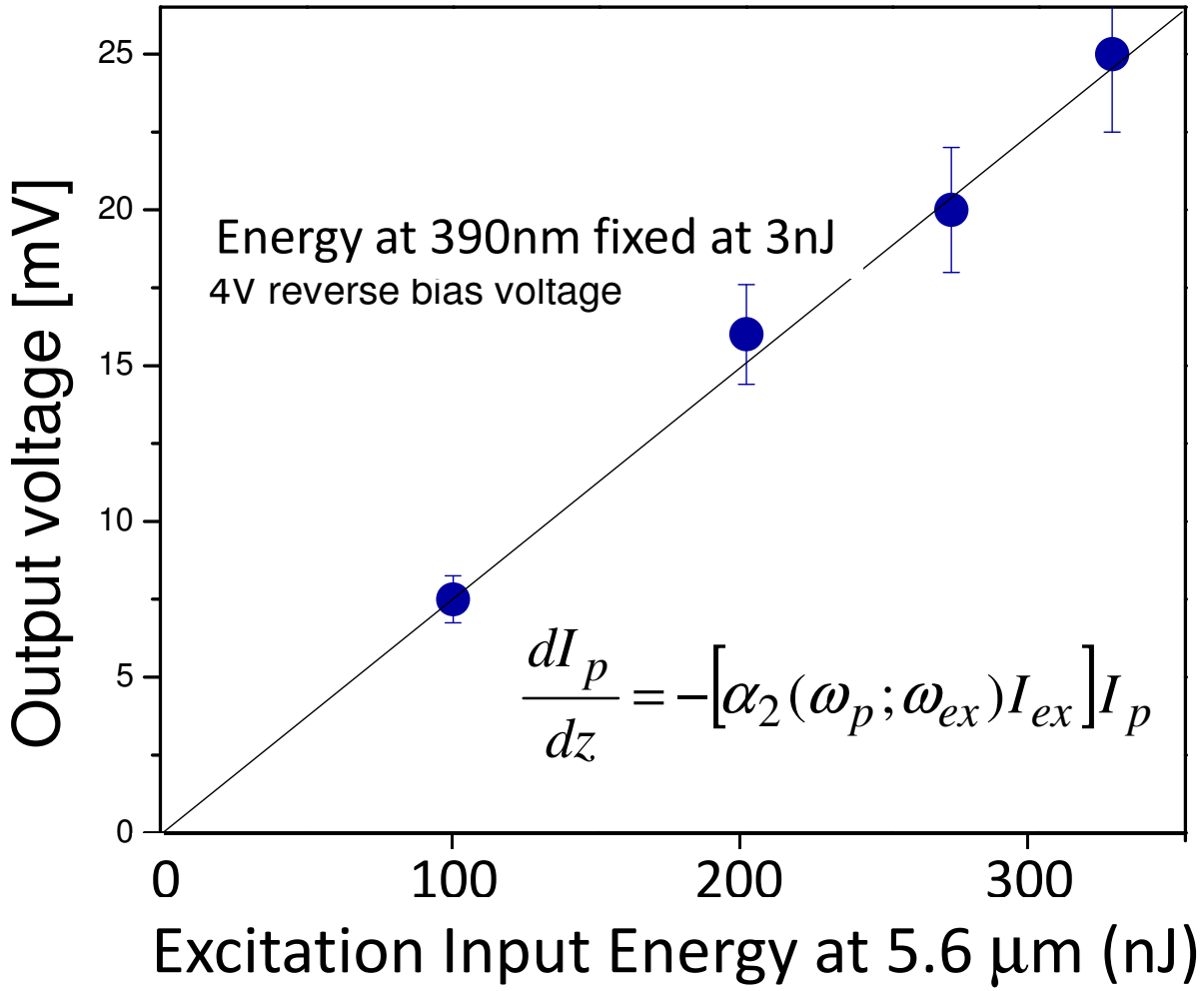

Pump at 390nm probe (i.e., detect) at IR

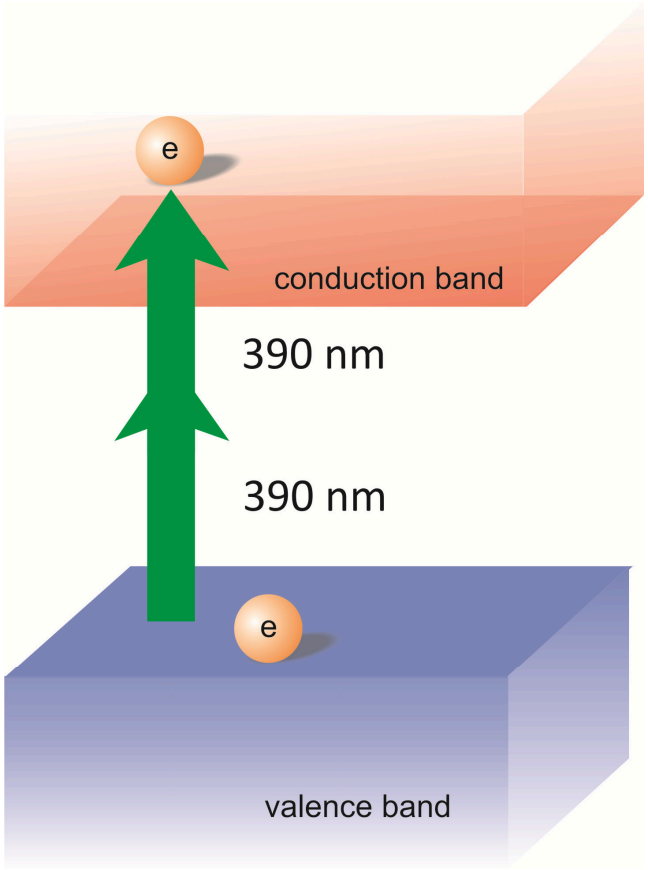

Quadratic dependence - Degenerate 2PA

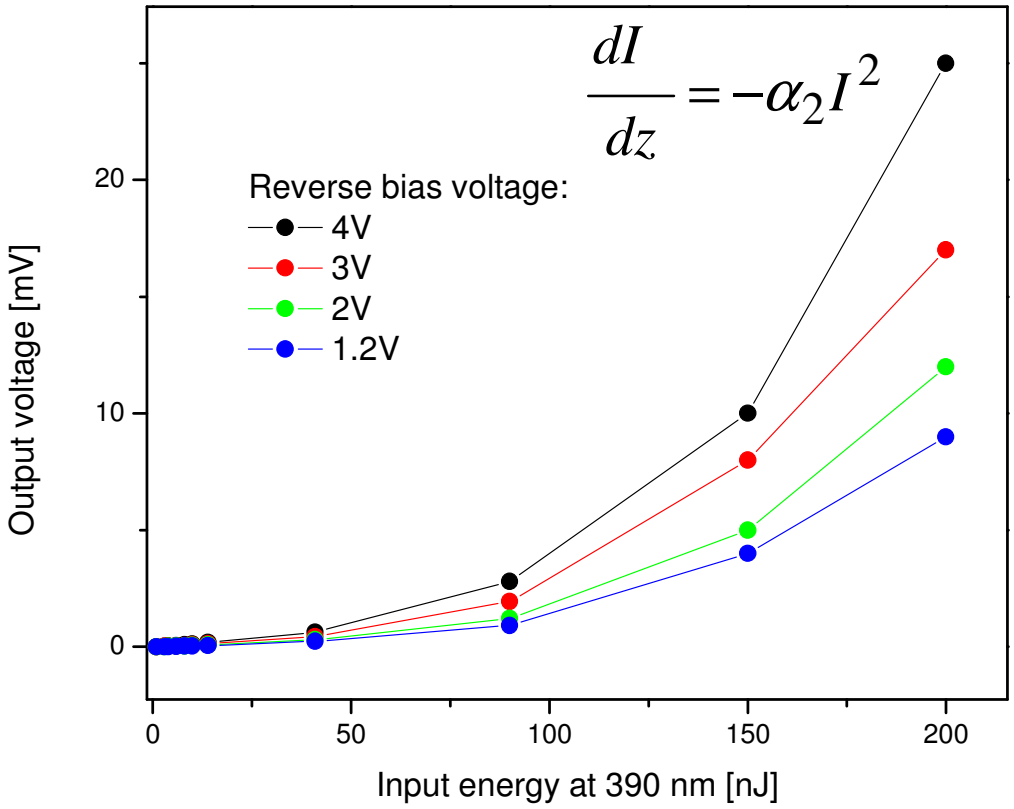

Detector response at 390 nm

For nondegenerate $F_2^{2PA}(x_1; x_2) = \frac{(x_1 + x_2 - 1)^{3/2}}{2^7 x_1 x_2^2} \left(\frac{1}{x_1} + \frac{1}{x_2} \right)^2$

IR Detection - Linear Power dependence

$$\frac{dI_p}{dz} = -\left[\alpha_2(\omega_p;\omega_{ex})I_{ex}\right]I_p$$

$$\frac{dI_{ex}}{dz} = -\alpha_2 I_{ex}^2$$

degenerate 2PA is ~20% of signal at 310nJ and 50% at 500nJ

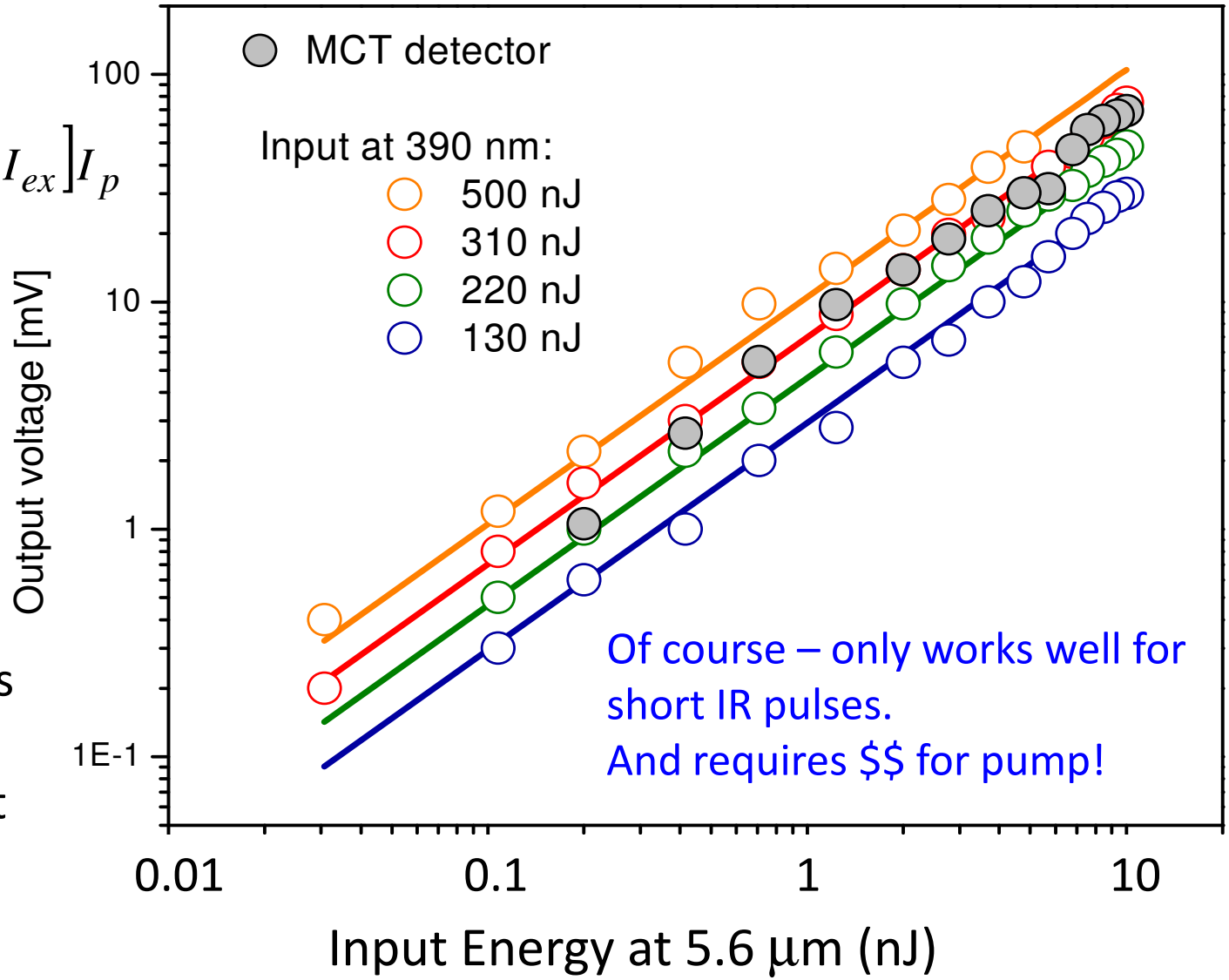

$$\frac{dI_p}{dz} = -\left[\alpha_2(\omega_p;\omega_{ex})I_{ex}\right]I_p$$ How high can we go before damage?

I find for Eg=3.278 eV, α_2=15.1 cm/GW for IR detection and 217 cm/GW for 390nm detection. 390nm is 97% of the gap energy and overall we are 3.75% above the gap. The correspondingα_2 for the degenerate case is 2.5cm/GW. The maximum possible degenerate 2PA for this is 2.51cm/GW, at x=0.5882, i.e. enhanced by 6.0 for IR detection and by 86 for 390nm detection.
If the GaN is 100 μm thick we absorb 13% of the IR for 1 GW/cm^2 and absorb 69% of the 390nm. Can we determine the thickness? Eventually sacrifice the detector? But first we could try hitting it harder! See just how large a response we can get before damage.
Then the question is what fraction of carriers does the detector capture . We probably gain some here compared to MCT. Perhaps there is some info on this??? We should also purchase some detectors if we haven't already (with known parameters – perhaps discuss with manufacturer?).

Other ?'s : The MCT detectivity is 7.4x larger while the responsivity is larger for GaN (>172 – can you pin this down any better?).
Do we have the thicknesses of all the samples?

Detector parameters GaN only

5900 nm pump (300nJ), 390 nm probe

Characteristic	Value	Units
Noise Equivalent Power, (NEP)	$8.5 \cdot 10^{-12}$	W/√Hz
Detectivity, D*	$5.8 \cdot 10^{9}$	cm·√Hz/W
Responsivity R	>0.033	A/W
Rise time, τ	0.183	μs

390 nm pump (310 nJ), 5900 nm probe

Characteristic	Value	Units
Noise Equivalent Power, (NEP)	$21 \cdot 10^{-12}$	W/√Hz
Detectivity, D*	$2.3 \cdot 10^{9}$	cm·√Hz/W
Responsivity R	>0.02	A/W
Response time, τ	0.183	μs

Irradiance
1 : 2.78

Detector parameters GaN vs MCT

MCT: 5900 nm probe only

Characteristic	Value	Units
Noise Equivalent Power, (NEP)	$23 \cdot 10^{-12}$	W/√Hz
Detectivity, D*	$1.7 \cdot 10^{10}$	cm·√Hz/ W
Responsivity R (zero amplification)	130 - measured 78 - specified	V/W
Detector area, d	4	mm
Impedance	50	Ohm
Amplifier gain	1000	

390 nm pump (310 nJ), 5900 nm probe

Characteristic	Value	Units
Noise Equivalent Power, (NEP)	$21 \cdot 10^{-12}$	W/√Hz
Detectivity, D*	$2.3 \cdot 10^{9}$	cm·√Hz/W
Responsivity R (zero amplification)	>172	V/W
Detector area, d	0.5	mm
Impedance	380000	Ohm
Amplifier gain	40	

GaN Detector Parameters

5600 nm pump (300nJ), 390 nm probe

Characteristic	Value	Units
Noise Equivalent Power, (NEP)	$8.5 \cdot 10^{-12}$	W/√Hz
Detectivity, D*	$5.8 \cdot 10^{9}$	cm·√Hz/W
Responsivity R	>0.033 >2400	A/W V/W

390 nm pump (310 nJ), 5600 nm probe

Characteristic	Value	Units
Noise Equivalent Power, (NEP)	$21 \cdot 10^{-12}$	W/√Hz
Detectivity, D*	$2.3 \cdot 10^{9}$	cm·√Hz/W
Responsivity R	>0.02	A/W
Responsivity R (zero amplification)	>172	V/W

MCT: 5600 nm

Characteristic	Value	Units
Noise Equivalent Power, (NEP)	$23 \cdot 10^{-12}$	W/√Hz
Detectivity, D*	$1.7 \cdot 10^{10}$	cm·√Hz/W
Responsivity R (zero amplification)	130 - measured 78 - specified	V/W

For IR, degenerate 2PA is ~20% of nondegenerate.
At higher pump, R~300V/W with 100% of degenerate 2PA. . .
(but easily separated)

GaN Detector Parameters

5600 nm pump (300nJ), 390 nm probe

Characteristic	Value	Units
Noise Equivalent Power, (NEP)	$8.5 \cdot 10^{-12}$	W/√Hz
Detectivity, D*	$5.8 \cdot 10^{9}$	cm·√Hz/W
Responsivity R (zero amplification)	>2400	V/W

390 nm pump (310 nJ), 5600 nm probe

Characteristic	Value	Units
Noise Equivalent Power, (NEP)	$21 \cdot 10^{-12}$	W/√Hz
Detectivity, D*	$2.3 \cdot 10^{9}$	cm·√Hz/W
Responsivity R (zero amplification)	>172	V/W

MCT: 5600 nm

Characteristic	Value	Units
Noise Equivalent Power, (NEP)	$23 \cdot 10^{-12}$	W/√Hz
Detectivity, D*	$1.7 \cdot 10^{10}$	cm·√Hz/W
Responsivity R (zero amplification)	130 - measured 78 - specified	V/W

For IR, degenerate 2PA is ~20% of nondegenerate.
At higher pump, R~300V/W with 100% of degenerate 2PA. . .
(but easily separated)

GaN Detector

Responsivity, R (zero amplification)

5600 nm pump (300nJ), 390 nm probe **R>2400 V/W**

390 nm pump (310 nJ), 5600 nm probe **R>170 V/W**

MCT: 5600 nm **R ~130 V/W measured**
78 V/W specified

For IR, degenerate 2PA is ~20% of nondegenerate.
At 500 nJ pump, R~300 V/W with degenerate 2PA ~100% . . .
(but easily separated)

Band gap energy of GaN detector

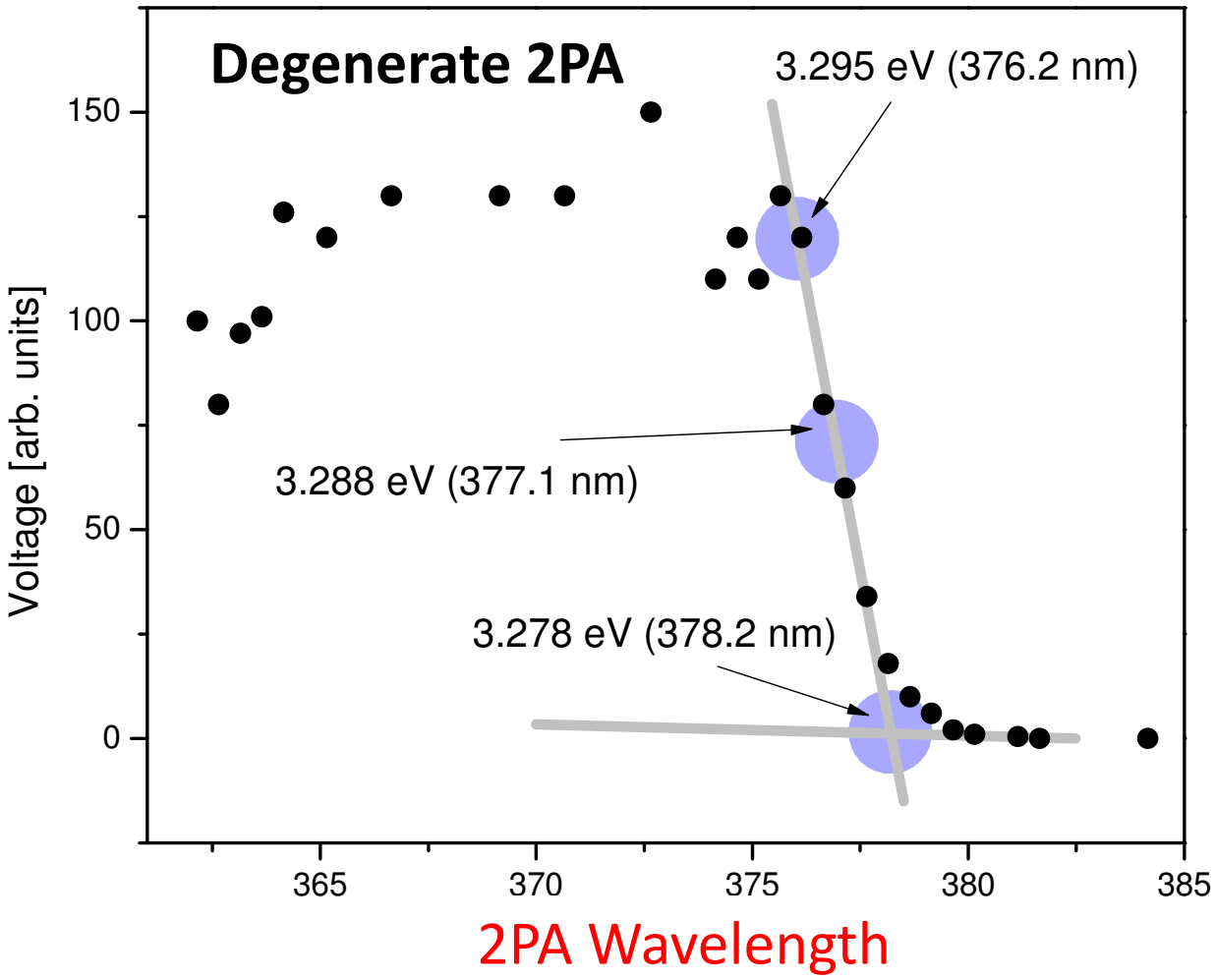

Bandwidth of UV pulse is 2.0nm ⟷

Calculate for Eg=3.278 eV

α_2=15cm/GW for IR detection

(x40)

α_2=220cm/GW for 390nm detection.

(x540)

α_2= 0.4cm/GW for the degenerate case is.

Nonlinear refraction

$$\Delta n(\omega;\Omega) = \frac{c}{\pi}\int_0^\infty \frac{\Delta\alpha(\omega';\Omega)}{\omega'^2-\omega^2}\,d\omega'$$

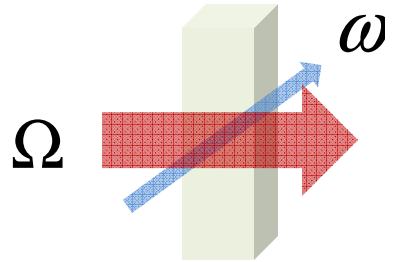

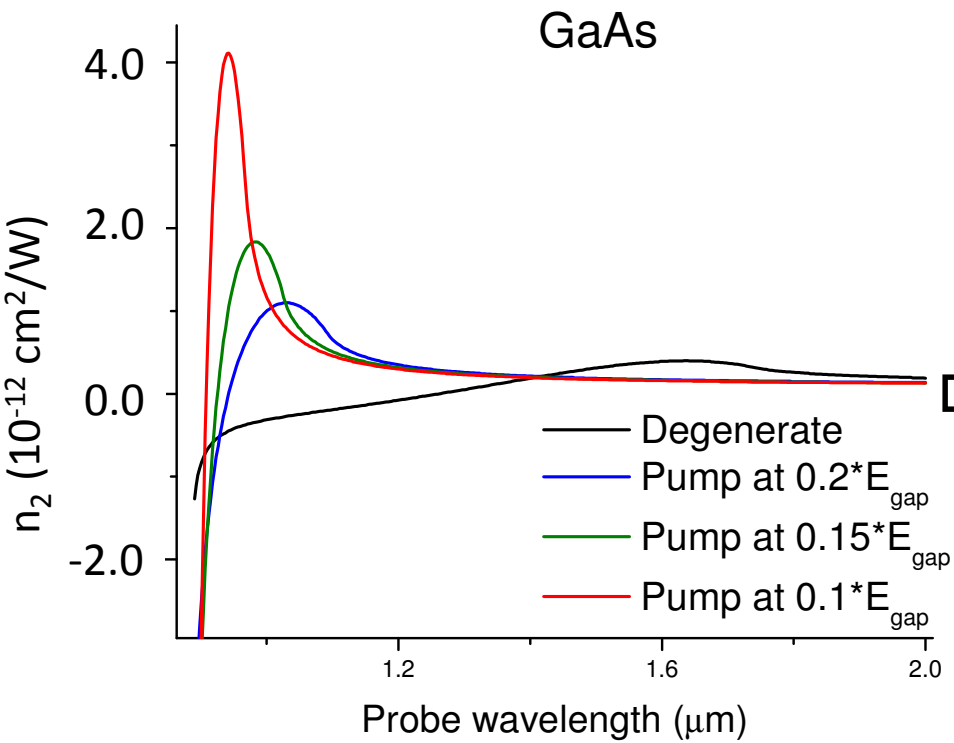

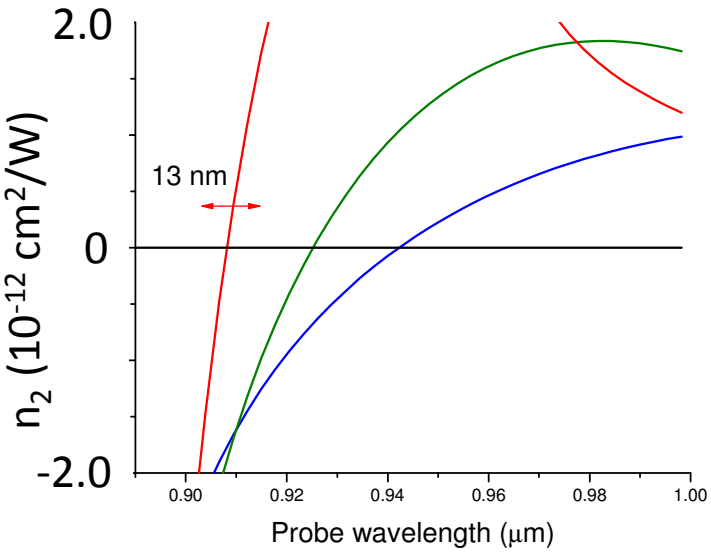

JQE 27, 1296-1309 (1991)

Conclusion

- Get orders of magnitude increase in 2PA with extreme nondegeneracy >10/1 in photon energy
  - ZnSe, CdTe, GaAs, ZnO, ZnS and GaN detector
- Use for detection of 390nm (below the gap) in GaN photodiode with 5.6 μm pump
- Use for detection of 5.6 μm in GaN photodiode with 390nm pump – as good as LN HgCdTe!
- Gated detection (sub-fs) of short pulses
- All-optical switching?
- 2-photon gain?

But requires $$$ laser

NLO Group at CREOL, UCF, 2009

Eric Van Stryland, Claudiu Cirloganu, Olga Przhonska, Peter Olszak, Trenton Ensley, Lazaro Padilha, Lihua Ye Davorin Peceli, Shima Fardad, Gero Nootz, Scott Webster, Amy Hand, Honghua Hu, David Hagan, Oliver Kahl.

Samples from: Seth Marder, Olga Przhonska, et al

Research scientists:
Scott Webster
Dmitri Fishman
Lazaro Padilha

David Hagan

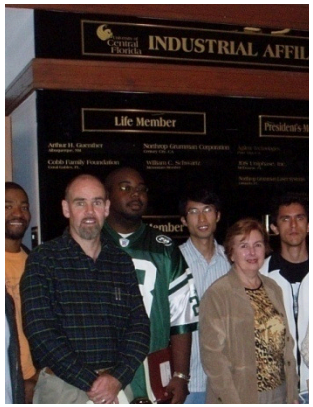

Olga Przhonska

Graduate students:
Honhua Hu
Gero Nootz
Peter Olszak
Trenton Ensley
Claudiu Cirloganu
Davorin Peceli
Oliver Kahl
Mathew Reichert
Himansu Pattanaik
Sihui He

Some People missing in photo

White-Light Continuum (WLC) Z-scan Technique for 2PA Measurements

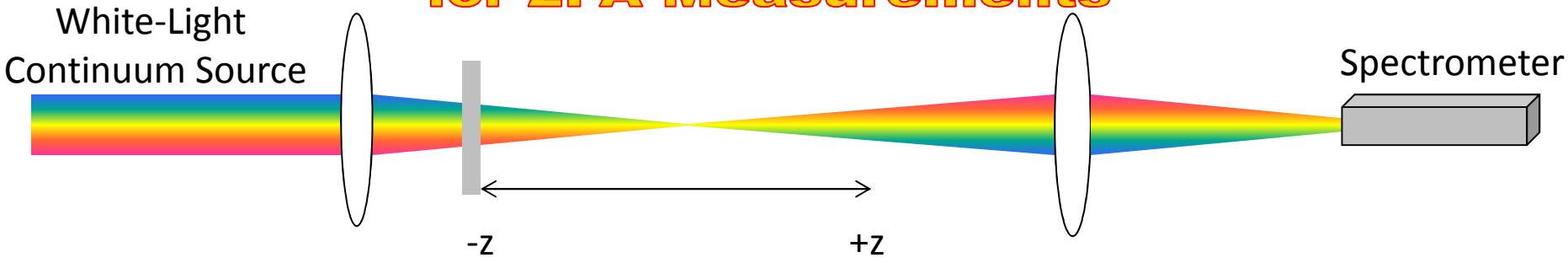

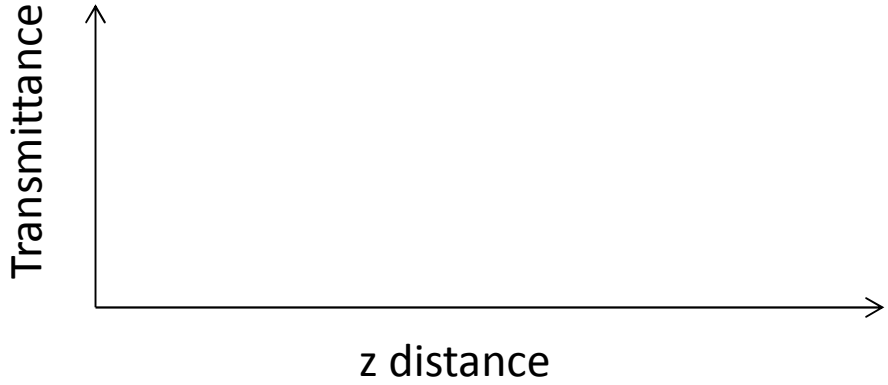

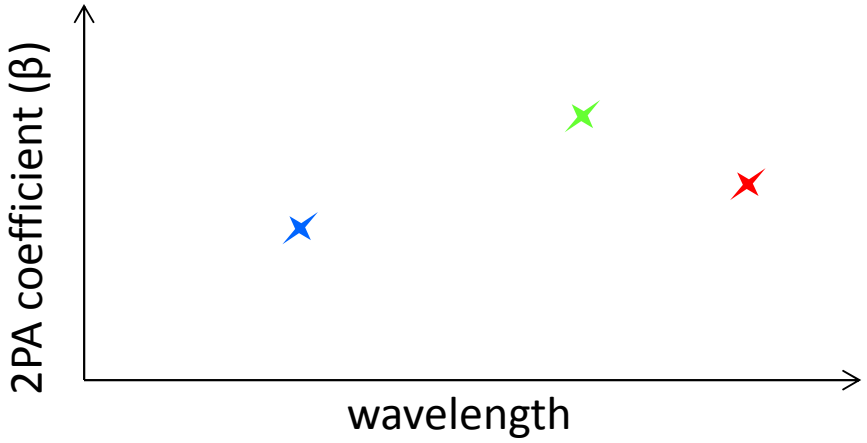

Problem!

Lots of wavelengths present in sample simultaneously.

WLC Z-scan

For degenerate nonlinearities it is necessary to select a narrow band of the WLC for each scan

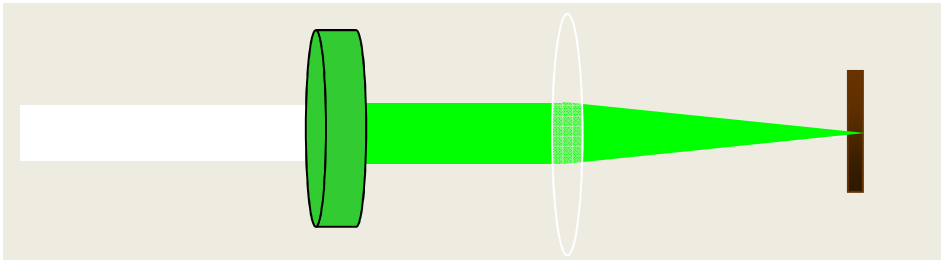

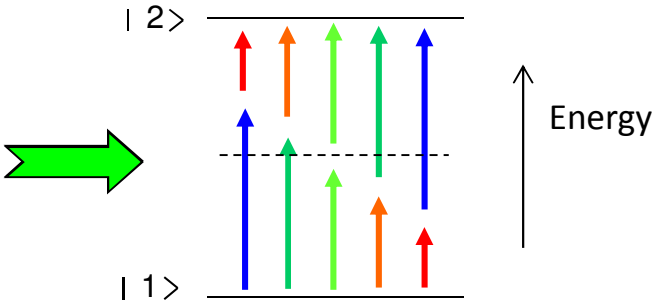

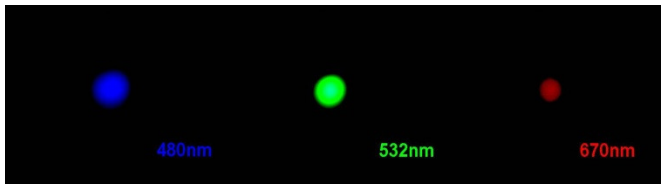

Seeding WLC generation

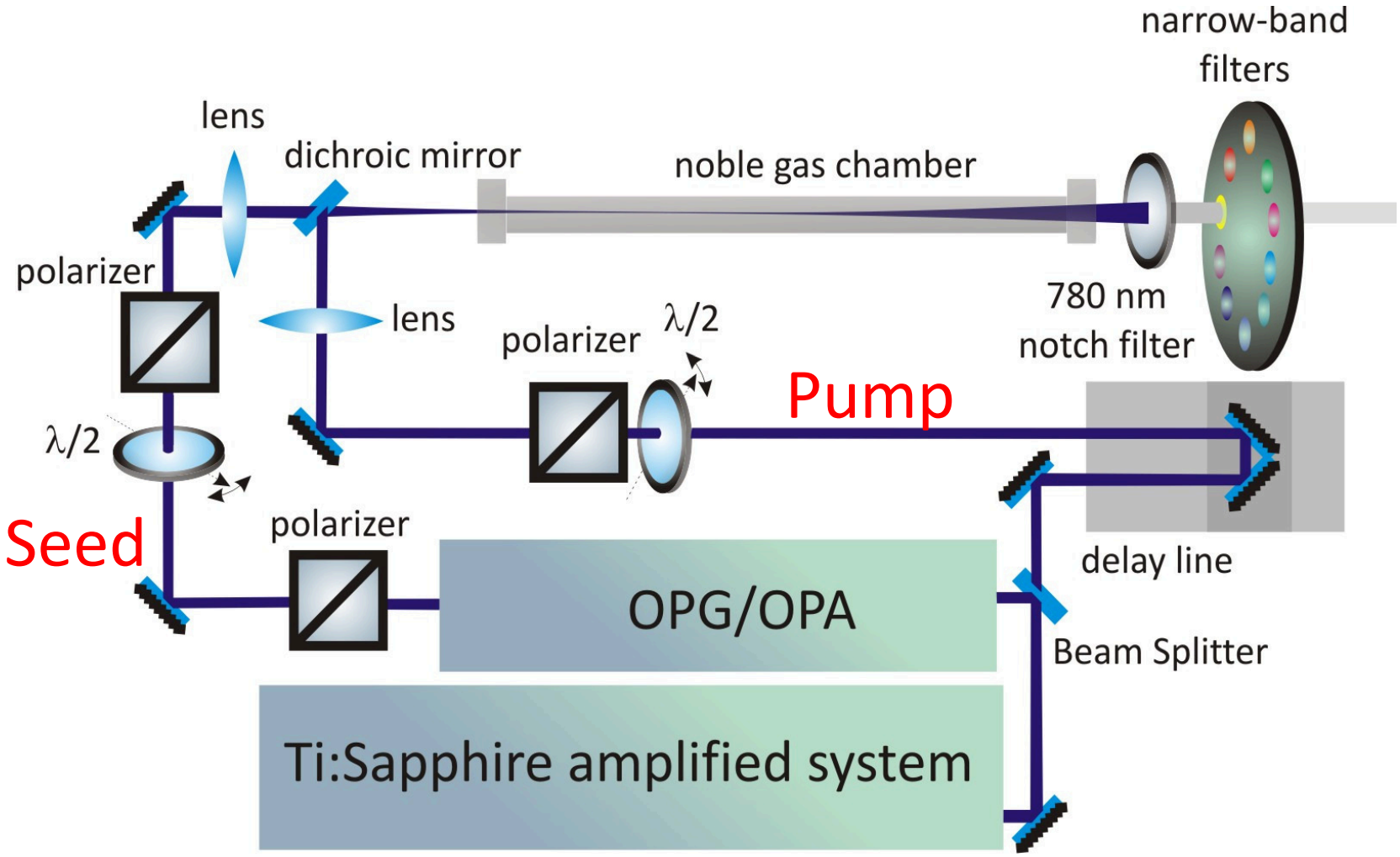

WLC Enhancement and Broadening

unseeded WLC (open black squares) (a) 600 nm seed

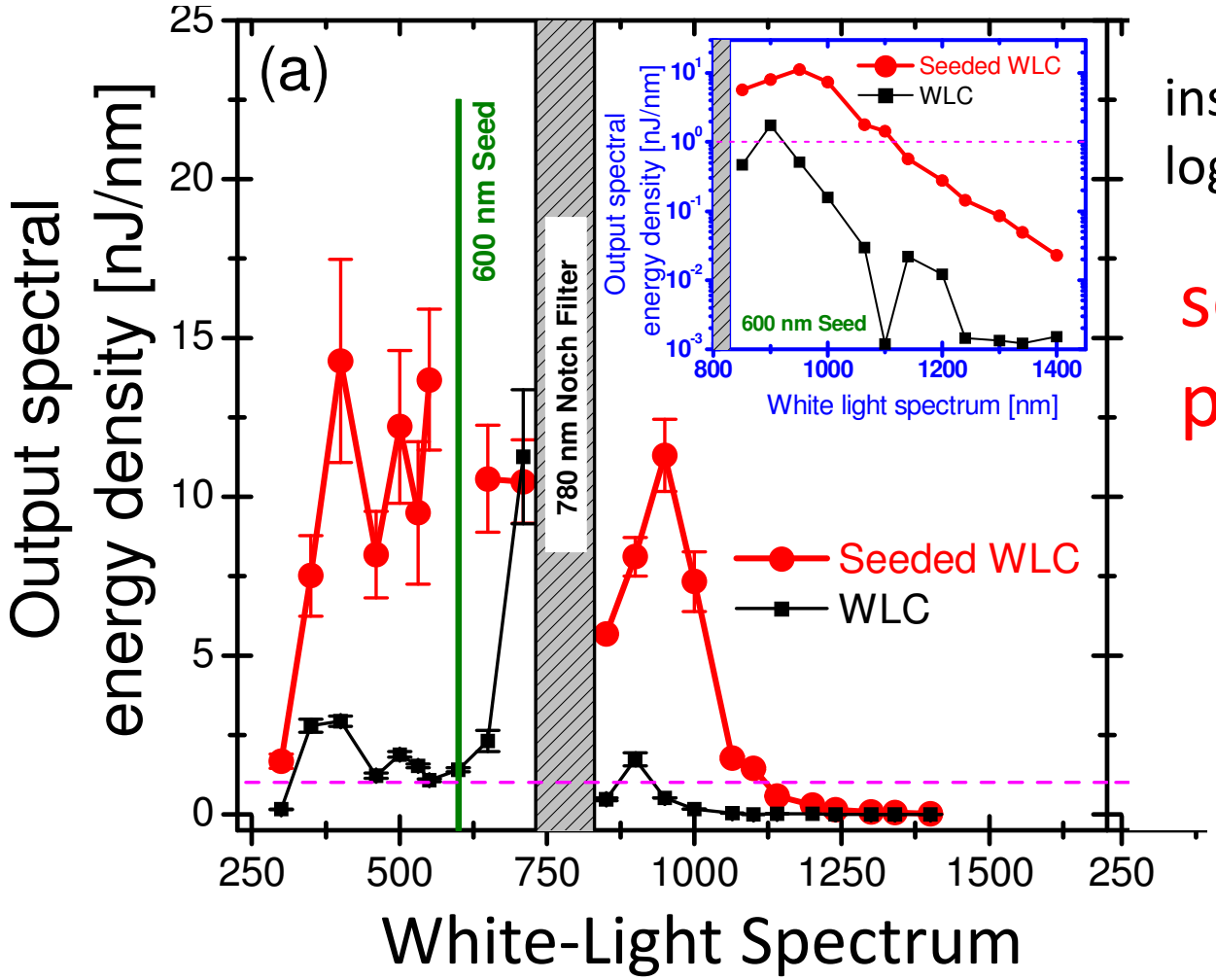

inset shows log scale

seed < 0.5% pump

WLC energy for different seed λ's.

Seed wavelength (nm)	WLC Energy Density @ 532 nm (nJ / nm)	WLC Energy Density @ 1000 nm (nJ / nm)	Total WLC Energy (μJ)
500	3.6 ± 1.2 (1.5)	3.9 ± 0.4 (0.17)	3.1 (1.2)
550	7.5 ± 2.1 (1.5)	2.3 ± 0.1 (0.17)	2.8 (1.2)
600	9.5 ± 2.2 (1.5)	7.2 ± 0.9 (0.17)	3.7 (1.2)
650	6.7 ± 1.2 (1.5)	14.2 ± 0.6 (0.17)	3.8 (1.2)
710	4.0 ± 0.7 (1.5)	1.1 ± 0.02 (0.17)	1.9 (1.2)
1150	2.5 ± 0.8 (1.5)	0.9 ± 0.3 (0.17)	1.3 (1.2)
1200	1.6 ± 0.2 (1.5)	0.3 ± 0.01 (0.17)	1.21 (1.2)
1240	1.5 ± 0.1 (1.5)	0.2 ± 0.01 (0.17)	1.3 (1.2)
1300	1.5 ± 0.1 (1.5)	0.17 ± 0.01 (0.17)	1.21 (1.2)

Unseeded WLC energy in parenthesis

Output energy at 532 ± 5 nm vs. 600nm seed energy.

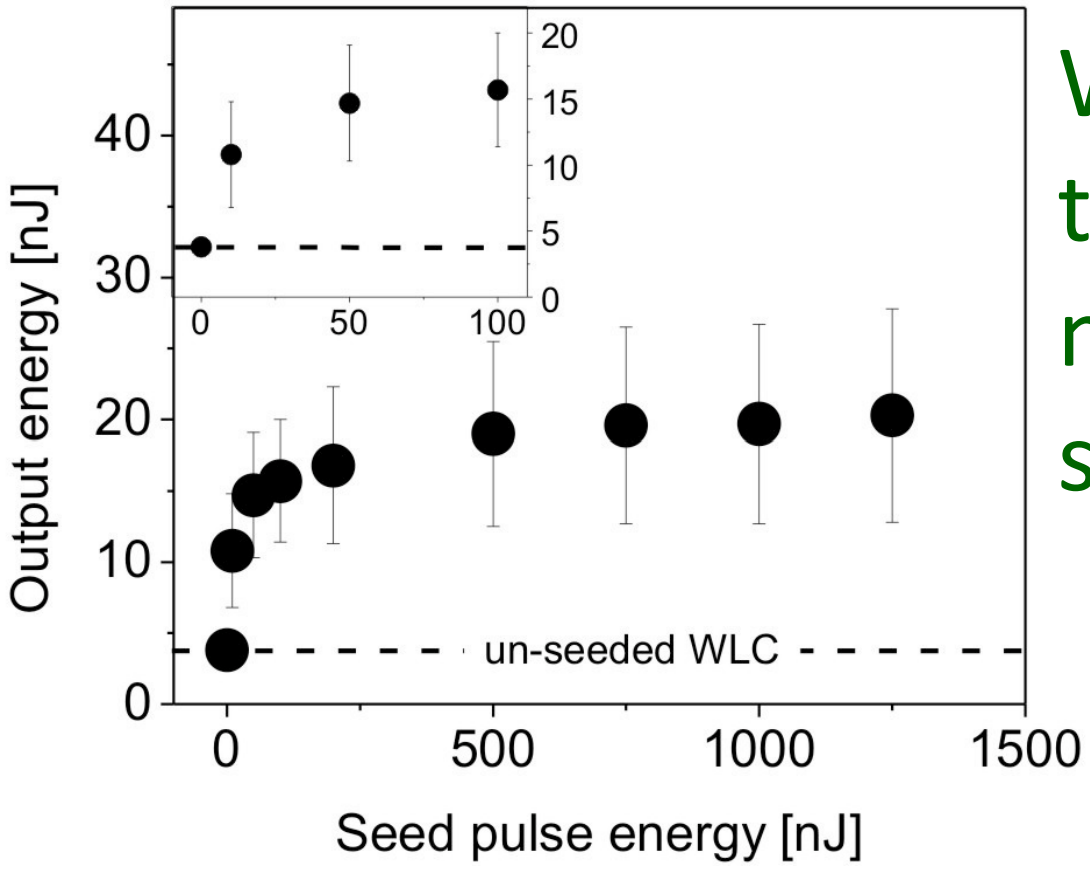

We can use this for nonlinear spectrometer

Enhancement observed for <10 nJ.

Pump ~ 0.5 mJ !

Stability at 1000Hz

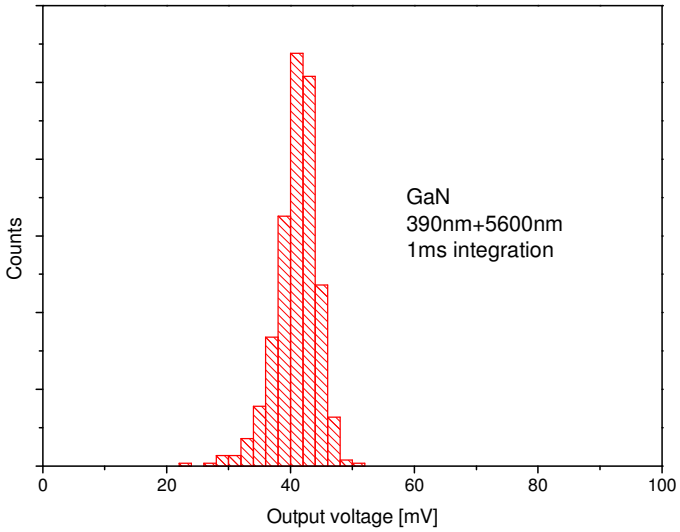

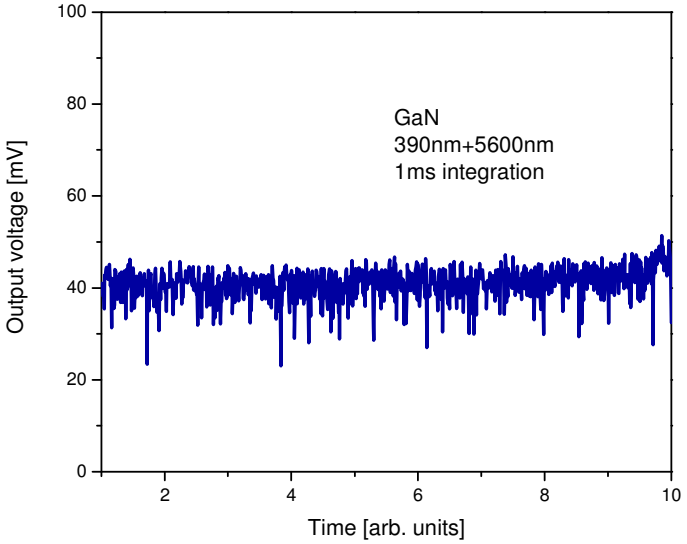

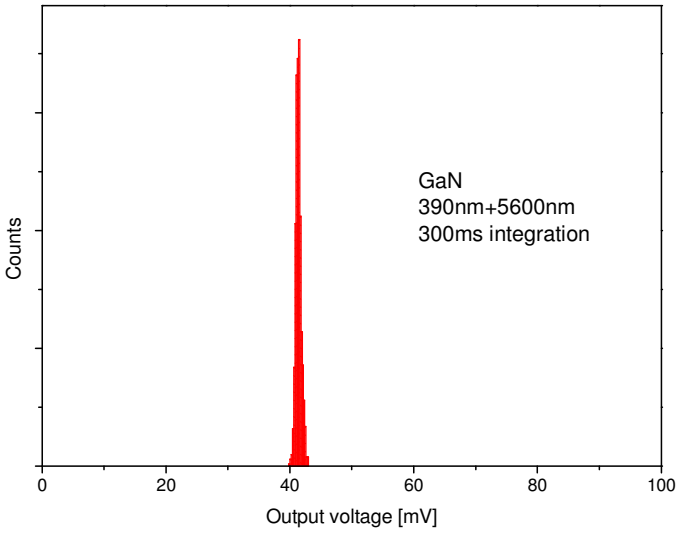

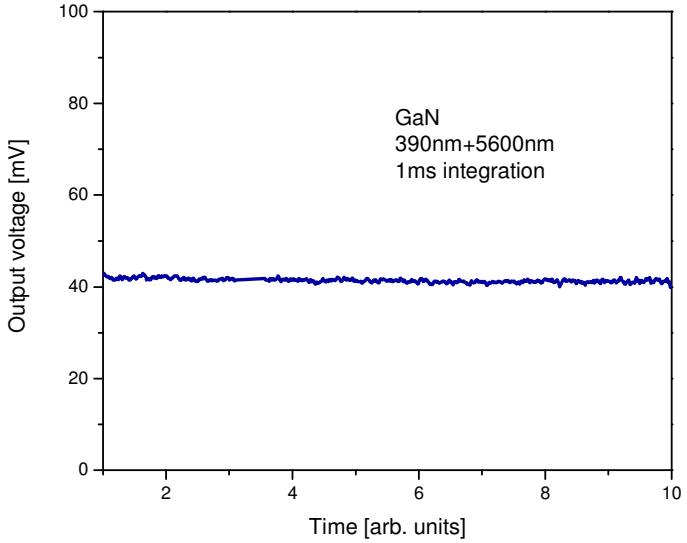

Stability at 1000Hz

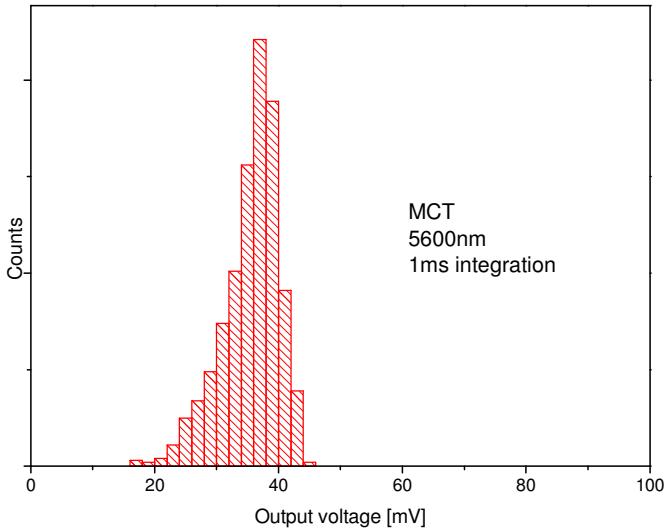

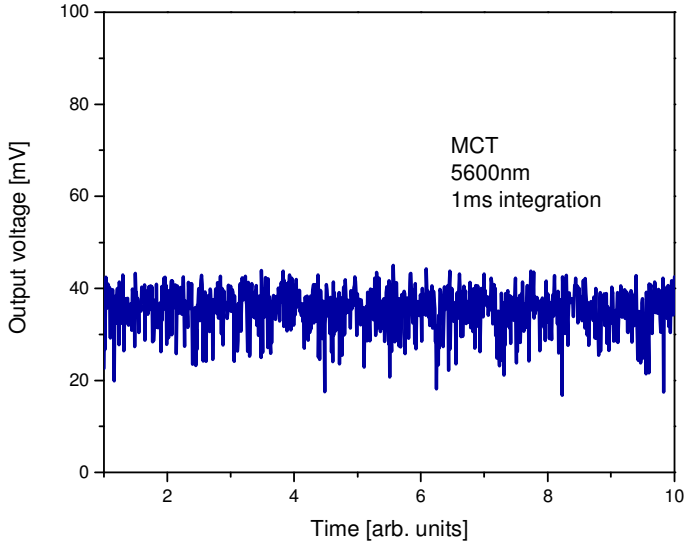

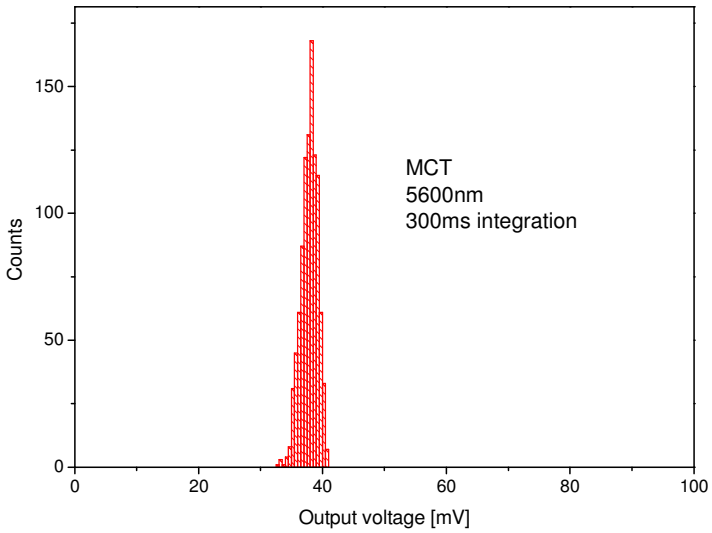

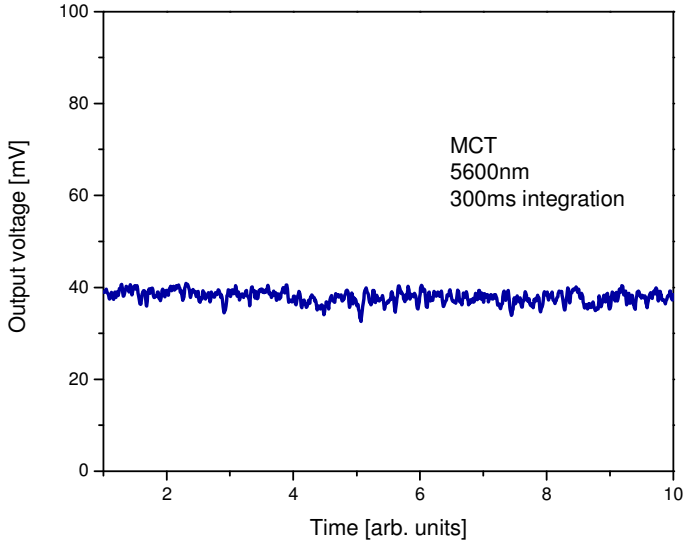

Response time

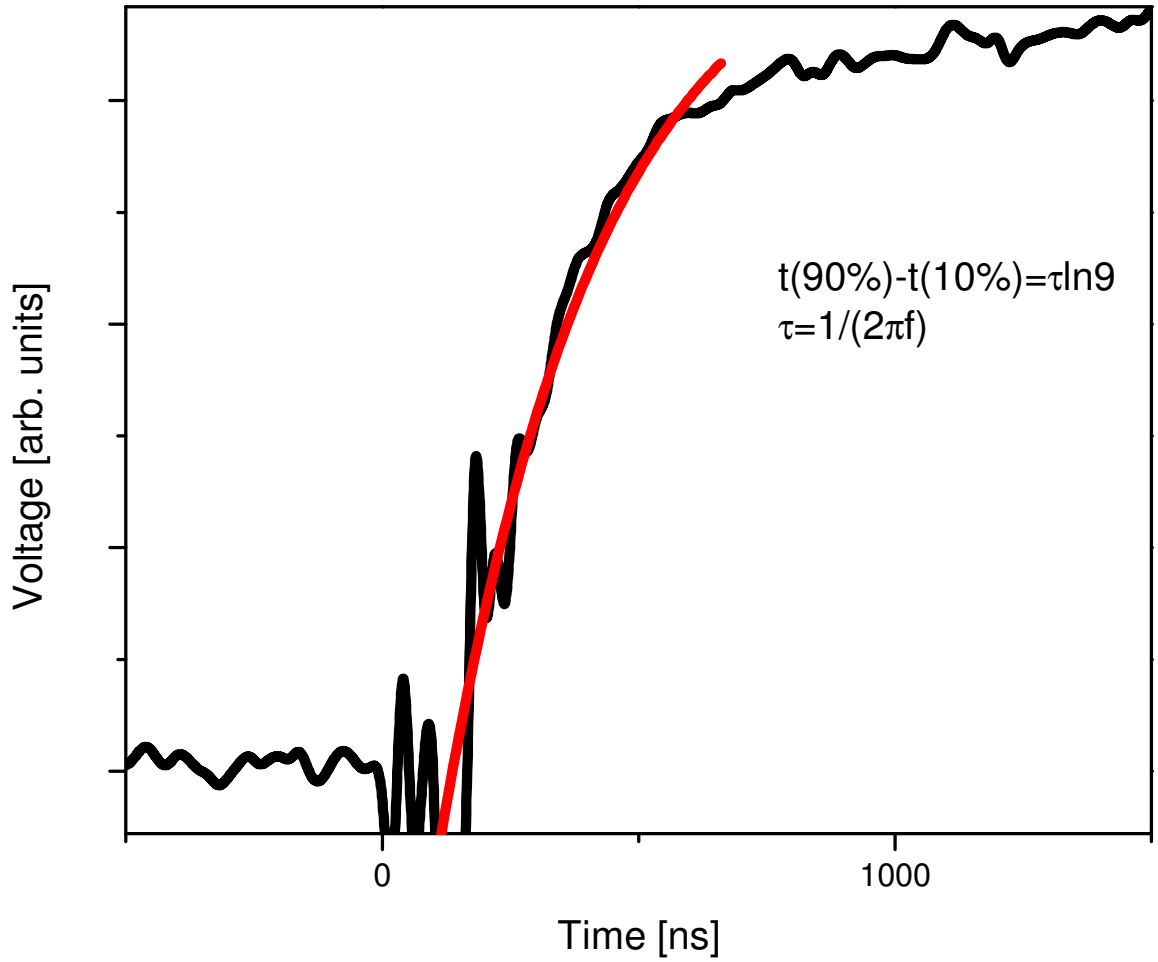

nature photonics

ARTICLES

PUBLISHED ONLINE: 7 AUGUST 2011 | DOI: 10.1038/NPHOTON.2011.168

Sensitive mid-infrared detection in wide-bandgap semiconductors using extreme non-degenerate two-photon absorption

Dmitry A. Fishman[1‡], Claudiu M. Cirloganu[1†‡], Scott Webster[1], Lazaro A. Padilha[1†], Morgan Monroe[1], David J. Hagan[1,2] and Eric W. Van Stryland[1,2]*

Identifying strong and fast nonlinearities for today's photonic applications is an ongoing effort[1]. Materials[2–5] and devices[6–9] are typically sought to achieve increasing nonlinear interactions. We report large enhancement of two-photon absorption through intrinsic resonances using extremely non-degenerate photon pairs. We experimentally demonstrate two-photon absorption enhancements by factors of 100–1,000 over degenerate two-photon absorption in direct-bandgap semiconductors. This enables gated detection of sub-bandgap and sub-100 pJ mid-infrared radiation using large-bandgap detectors at room temperature. Detection characteristics are comparable in performance to liquid-nitrogen-cooled HgCdTe (MCT) detectors. The temporal resolution of this gated detection by two-photon absorption is determined by the gating pulse duration.

Semiconductors are excellent materials for photonic switching because of their large third-order nonlinearities, and have been the subject of extensive studies, both experimental and theoretical[10,11]. These nonlinearities, both refractive and absorptive, have been successfully modelled and experimentally verified in many material-wavelength combinations[12–14]. However, little attention has been paid to theoretical predictions for the case where the input wavelengths are vastly different. Consequently, before the present study, no efforts had been made to study extreme non-degenerate two-photon absorption (ND-2PA) experimentally. A theoretical treatment of ND-2PA in direct-bandgap semiconductors using two parabolic bands has shown that ND-2PA may be expressed by[15]

$$\frac{\mathrm{d}I_1}{\mathrm{d}z} = -2\alpha_2(\omega_1;\omega_2)I_2I_1$$

$$\text{with} \qquad \alpha_2(\omega_1;\omega_2) = K\frac{\sqrt{E_\mathrm{p}}}{n_1n_2E_\mathrm{gap}^3}F_2\left(\frac{\hbar\omega_1}{E_\mathrm{gap}};\frac{\hbar\omega_2}{E_\mathrm{gap}}\right) \qquad (1)$$

where

$$F_2(x_1;x_2) = \frac{(x_1+x_2-1)^{3/2}}{2^7x_1x_2^2}\left(\frac{1}{x_1}+\frac{1}{x_2}\right)^2$$

$\alpha_2(\omega_1;\omega_2)$ is the ND-2PA coefficient for optical frequencies $\omega_{1,2}$ and their associated irradiances $I_{1,2}$, E_p is the Kane energy parameter, E_gap is the bandgap energy, $n_{1,2}$ are the refractive indices, and K is a material independent parameter.

From the energy denominators in F_2, 2PA is expected to increase drastically if either ω_1 or ω_2 becomes small. As 2PA requires $\hbar\omega_1 + \hbar\omega_2 \geq E_\mathrm{gap}$, this means that 2PA increases with the ratio of photon energies. This can be qualitatively understood by noting that the allowed–forbidden transition scheme in perturbation theory dominates 2PA in direct-bandgap semiconductors, as shown by Wherrett[16]. Thus, the smaller energy photon is almost resonant to the intraband (or self) transition. The limits to this enhancement are dictated by the linear absorption of the higher energy photon as it approaches the linear absorption resonance. Hence, the degenerate 2PA (D-2PA) case gives the minimum 2PA, and can only be enhanced by using the E_gap^{-3} dependence in equation (1). This results in the use of narrow-bandgap semiconductors and thus mid-infrared (MIR) wavelengths. This E_gap^{-3} dependence was verified experimentally, revealing D-2PA coefficients for narrow-bandgap semiconductors such as InSb that are three orders of magnitude larger than for large-bandgap semiconductors such as ZnSe[12,13,17]. The use of extremely non-degenerate photons in wide-bandgap materials results in 2PA coefficients similar to those obtained using degenerate photons in narrow-bandgap materials. These enhancements observed for extreme ND-2PA should also apply to other material systems provided that the linear absorption band edge is sufficiently sharp[18–20].

The large increase in 2PA for extreme non-degenerate configurations can be applied in a variety of ways. One of the most straightforward effects of the simultaneous absorption of two largely different photon energies is the promotion of a free carrier into the conduction band. One can monitor the photo-generated charges in such experiments using a 'gating' pulse, where this pulse can be composed of either high- or low-energy photons. We use the word 'gating' because this intense pulse essentially turns the detector on to monitor the intensity of the 'signal' pulse. If the gating pulse consists of low-energy photons, such experiments enable high-sensitivity detection of sub-bandgap-energy photons. Alternatively, a gating pulse comprising high-energy photon pulses (but still below the band edge) allows the detection of MIR photons using a large-bandgap semiconductor.

[1]CREOL, the College of Optics & Photonics, University of Central Florida, 4000 Central Florida Blvd., Orlando, Florida 32816-2700, USA, [2]Department of Physics, University of Central Florida, 4000 Central Florida Boulevard, Orlando, Florida 32816, USA; †Present address: COPE, Center for Organic Photonics and Electronics, School of Electrical and Computer Engineering, Georgia Institute of Technology, Atlanta, Georgia 30332, USA, Los Alamos National Laboratory, PO Box 1663, Los Alamos, NM 87545, USA (L.A.P.); ‡These authors contributed equally to this work. *e-mail: ewvs@creol.ucf.edu

Figure 1a shows the detection of femtosecond pulses at 390 nm (3.18 eV) by a conventional GaN detector with $E_{gap} = 3.28$ eV (direct output voltage) using MIR gating pulses at 5.6 μm (6.7% of E_{gap}) (see Supplementary Information for details). The signal, which is proportional to the photo-generated carrier density N, is linear in both the MIR and ultraviolet (UV) beam irradiances, and is given by

$$\frac{dN}{dt} = 2\alpha_2(\omega_s;\omega_g)I_gI_s/\hbar\omega_s = 2\alpha_2(\omega_g;\omega_s)I_gI_s/\hbar\omega_g = K\frac{\sqrt{E_p}}{n_1n_2E_g^4}F_2^{symm}\left(\frac{\hbar\omega_s}{E_g};\frac{\hbar\omega_g}{E_g}\right)2I_sI_g \quad (2)$$

with $F_2^{symm}(x_1;x_2)$ given by

$$F_2^{symm}(x_1;x_2) = \frac{(x_1+x_2-1)^{3/2}}{2^7(x_1x_2)^2}\left(\frac{1}{x_1}+\frac{1}{x_2}\right)^2$$

where I_s, $\hbar\omega_s$ and I_g, $\hbar\omega_g$ are irradiances and photon energies of signal and gating pulses, respectively. We introduce $F_2^{symm}(x_1;x_2)$ to explicitly show that although the 2PA coefficients are not symmetric in the two input frequencies, the detected carrier density is symmetric in these frequencies, so the signal enhancement is the same for gated detection of MIR and UV light.

The measured detector responsivity R (5.6 μm; @ 0.5 GW cm^{-2}) is >0.034 A W^{-1} (additional detector parameters are found in the Supplementary Information). These results are linearly dependent on the irradiance at 5.6 μm (~0.5 GW cm^{-2}) as the effective 'linear' absorption is $\alpha_2(\omega_s;\omega_g)I_g$. Corresponding 730 nm pulses of approximately the same pulse energy as the UV pulses yield a D-2PA signal voltage that is nearly three to four orders of magnitude smaller (indicated by the results in Fig. 1a).

We can also detect weak 5.6 μm by increasing the irradiance of the 390 nm pulses to act as a gate. Thus a wide-bandgap semiconductor ($E_{gap} = 3.28$ eV) can be used for the detection of MIR light of photon energy 0.22 eV (5.6 μm). However, the cross absorption term is now accompanied by the D-2PA of the 390 nm pulses, $\alpha_2(\omega_g;\omega_g)$,

$$dN/dt = \alpha_2(\omega_g;\omega_g)I_g^2/2\hbar\omega_g + 2\alpha_2(\omega_s;\omega_g)I_gI_s/\hbar\omega_s \quad (3)$$

where the signal is 5.6 μm and the gate is 390 nm. The calculated values of D- and ND-2PA, $\alpha_2(\omega_{390nm};\omega_{390nm})$, and $\alpha_2(\omega_{5600nm};\omega_{390nm})$, $\alpha_2(\omega_{390nm};\omega_{5600nm})$ are 2.2 cm GW^{-1}, 17 cm GW^{-1}, and 240 cm GW^{-1}, respectively. This gives a ratio for the IR gating of 110, whereas the measured ratio is 95. The D-2PA signal can be suppressed for repetitive pulses using the modulation of the MIR pulses and lock-in detection, easily allowing for the detection of sub-100 pJ pulse energies at 5.6 μm (see Supplementary Information). This is shown in Fig. 1b, where we demonstrate 5.6 μm detection using a GaN detector at room temperature. We compare the signals with gated detection in GaN using several 390 nm pulse energies with the output voltage from a conventional liquid-nitrogen-cooled mercury cadmium telluride (MCT) detector. The results show comparable or even superior performance for the investigated detectors (see Supplementary Information for details).

There are a few salient facts that need to be stressed regarding these experiments. As seen in Fig. 1, we are able to directly compare signals obtained when measuring MIR wavelengths using either one-photon or two-photon processes. It is obvious that when using a linear process, the responsivity depends solely on the overall linear absorption of the material used (that is, αL), where α is the linear absorption coefficient and L is detector element thickness. In the ND-2PA case, the effective absorption coefficient is $2\alpha_2 I_g$. In both cases we desire the overall thickness to be greater than the absorption depth. We estimate for the experiments demonstrated here that we are well away from this limit (~2% loss in the active detector region), and there is considerable optimization that can be performed. Also, because we do not

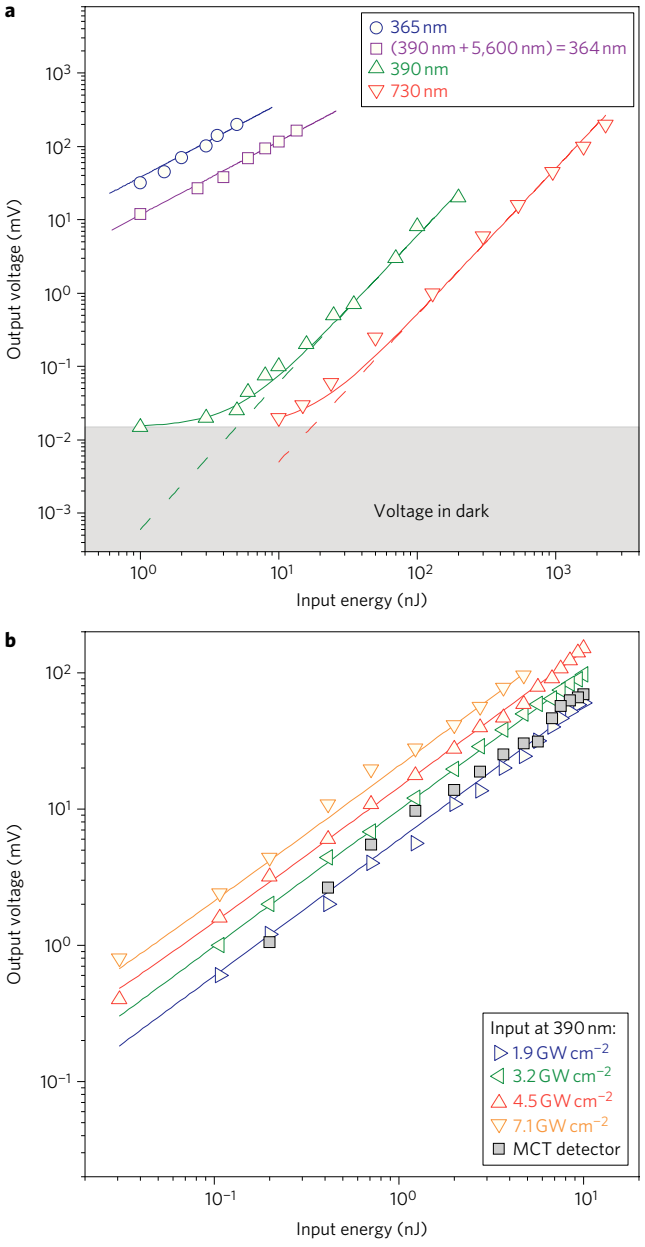

Figure 1 | Mid-IR detection using a UV photodiode. a, Log–log plot of the output voltage of a GaN diode versus 390 nm (3.18 eV, 100 fs) input signal energy in the presence of temporally overlapped, 300 nJ, 215 fs, 5.6 μm (0.22 eV) gating pulses. Also shown are outputs versus 365 nm (linear response) (100 fs), 390 nm without the gating pulses and signal from D-2PA of 730 nm (1.70 eV, 110 fs) pulses. Lines are fits to either slope 1 (for a linear dependence) or 2 (for a quadratic dependence) with ~15 μV of dark voltage. **b**, Log–log plot of the output voltage of a GaN diode versus 5.6 μm (215 fs) input signal energy in the presence of temporally overlapped 390 nm gating pulses (100 fs) of various energies. The grey filled squares show data for the MCT detector. See Supplementary Information for detector specifications.

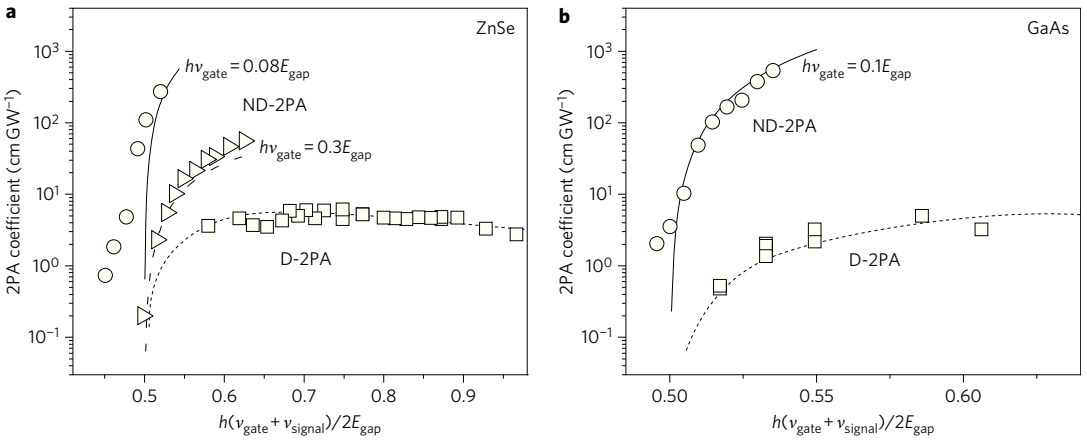

Figure 2 | Extreme ND-2PA in semiconductors. a, Femtosecond pump (gate)–probe (signal) results: D- and ND-2PA coefficient of ZnSe ($E_{gap} = 2.67$ eV) versus the sum of pump and probe photon energies normalized to the bandgap: theory (lines). **b**, Picosecond pump–probe results: D- and ND-2PA coefficients of GaAs ($E_{gap} = 1.42$ eV).

require high-speed detection, thick materials including waveguide geometries could be helpful.

In 2PA detection one preserves the signal linearity while having direct control of the responsivity via the gating pulse irradiance $R = A{\cdot}I_g$, where $A = 7.1 \times 10^{-12}$ cm^2 A W^{-2} for the 390 nm gating pulse ($A = 6.8 \times 10^{-11}$ cm^2 A W^{-2} for the MIR gating pulse). This offers flexibility for some applications that can outweigh the necessity of having a gating pulse. One can then measure pulsed low-energy MIR radiation using room-temperature detectors with a user-controlled responsivity. Also, even though the results of these experiments are related to the particular material and wavelength pair, the same approach can be used to measure any other pair of wavelengths using a material with appropriate bandgap energy. The bandwidth is determined by a trade-off with the 2PA enhancement, as will be seen from the transmittance experiments described in the next paragraph. One possible concern is the current created through direct D-2PA. However, the D-2PA is not enhanced; therefore, for practical applications the irradiance levels needed for the gate pulse should not lead to saturation effects. For MIR detection, the D-2PA of the gating pulse appears as a background signal. In our experiments, amplitude noise on the gating laser pulse dominates the contributions to noise. Noise from the gated signal is linear in the gate irradiance, whereas the degenerate 2PA noise is quadratic in the gate irradiance. There is therefore a trade-off between responsivity, which is linear in the gate irradiance, and this noise, which can have linear or quadratic contributions (Fig. 1). This is analogous to having a 'noisy' detector electronic amplifier; however, this 'noise' is measurable and could in principle be calibrated out. For this reason, we do not quote a noise-equivalent power or D^* for this detection scheme. However, the minimum detectable energy (Fig. 1b) is ~20 pJ, whereas for MCT the minimum detectable energy is ~200 pJ (for details of detector parameters, such as pre-amplifier and transimpedance gain, see Supplementary Information). This difference is in large part due to the fact that we can use modulation techniques with the ND-2PA gated detection scheme.

An alternative to this new detection method is frequency upconversion using second-order nonlinear optical materials in which IR and visible/near-IR photons are summed to yield photons of sufficient energy to be used with high-quantum-efficiency detectors such as silicon[21–23]. The primary similarity is that both detection schemes result in photocarrier densities proportional to the product of gate and signal irradiances. However, upconversion requires phase-matched second-order nonlinear materials. After years of development, it has resulted in near-unity detection quantum efficiencies[24–26]. The ND-2PA method demonstrated here is considerably simpler, because the detector element itself is the nonlinear material and no phase-matching is required; however, considerable research and development is necessary for it to reach its ultimate limits.

To provide a quantitative picture we performed detailed transmission studies of the direct-bandgap semiconductors ZnSe and GaAs using various photon energy ratios and picosecond and femtosecond pulses. In these experiments, the transmittance of weak visible pulses was monitored in the presence of intense MIR pulses (see Supplementary Information). 2PA coefficients for ZnSe and GaAs at different photon energy ratios are presented in Fig. 2a and b, respectively. Large enhancements of ND-2PA values versus D-2PA values were obtained, by as much as 270× in ZnSe (photon energy ratio up to 12.5, Fig. 2a) and 127× in GaAs (photon energy ratio of 10, Fig. 2b). For these semiconductors, the experimental results agree with theory, except for deviations observed when the sum of photon energies is less than the bandgap. This exception is probably due to absorption in the Urbach tail[27].

This greatly enhanced 2PA should enable many new opportunities beyond detection, such as all-optical switching[28] using microring resonators[29], and waveguides[30] with direct-bandgap semiconductors such as GaAs[31], where the resonating light is just below the band edge. Here the cavity Q can be easily spoiled using IR pulses via ND-2PA. Gated detection has also been suggested for quantum detectors[32,33]. The enhancement noted here makes these much more attractive. Finally, we note that this very large enhancement of 2PA in the case of non-degenerate photons implies that two-photon gain[34] should show a similar enhancement with non-degeneracy. Experiments have shown two-photon emission of very non-degenerate photons.

The application to sub-bandgap detection in the commercial GaN detector studied here is far from optimized for the detection of extremely non-degenerate photons. For example, the ND-2PA could be significantly increased by using a thicker detector element to efficiently absorb the radiation. The intrinsic detector temporal response is irrelevant, because the speed of detection is determined by the gating pulsewidth. In addition, an ultralow-noise optical comb source could be used as the gating source, which would greatly improve the signal-to-noise ratio[35].

Methods

The experimental ND-2PA data presented in this Article were taken in a standard pump–probe non-collinear geometry with a small angle (~10°) between the pump and probe beams, using either picosecond or femtosecond pulses. A Ti:sapphire

laser system (ClarkMXR, CPA 2010) was used as a source of femtosecond pulses, producing ~1.4 mJ, ~150 fs (FWHM), 780 nm pulses at a repetition rate of 1 kHz. The output of the laser system was divided into two pulses by a beamsplitter. A portion of the 780 nm light was used to pump an optical parametric generator/amplifier (OPG/A, TOPAS-800, Light Conversion) to generate MIR pulses. For the near-IR (1.7–2.5 μm, used for transmission experiments) an idler pulse was used, but for longer wavelengths we used difference frequency generation (DFG) of signal and idler pulses. The irradiance of the IR pulses was controlled by a calibrated pair of BaF_2 wire-grid polarizers (Specac). The remainder of the 780 nm output was temporally delayed and used either to generate a weak white-light continuum (WLC, used as a probe for bulk semiconductor measurements) or to generate an intense second harmonic (390 nm) and used as a strong pump pulse for gated detector measurements. WLC was generated either in water (1 cm cell) or in a 2-mm-thick piece of CaF_2. Individual wavelengths were selected from the WLC using a set of narrow band-pass interference filters (Melles Griot, CVI) with a spectral bandwidth of ~8 nm (FWHM). The temporal width of the spectrally filtered pulses was between 140 fs and 160 fs, as verified by autocorrelation measurements. Pulsewidths in the femtosecond MIR were determined from cross-correlation measurements to be ~215 fs (FWHM). In all ND-2PA experiments the MIR was modulated using a mechanical chopper at 283 Hz, synchronized with the repetition rate from the Ti:sapphire laser. A lock-in amplifier was then used to record the signals. This MIR modulation ensured that D-2PA did not contribute to the lock-in output.

A similar set-up was used for the picosecond experiments. A mode-locked Nd:YAG laser system (EKSPLA) produced ~30 ps (FWHM) pulses of 110 mJ at 1,064 nm and a repetition rate of 10 Hz. The fundamental pulses were converted to the third harmonic at 355 nm, which then pumped a lithium triborate, LiB_3O_5 (LBO)-based OPG/OPA. The MIR pump pulses were obtained using a DFG process, mixing 1,064 nm output from the laser and the idler pulse from a second similar OPG/OPA. The probe beam had a maximum energy of a few nanojoules and a spot size smaller than that of the pump, as measured by knife-edge scans. This assured an irradiance in the probe beam smaller (by at least a factor of 100) than that of the pump beam. This caused minimal losses from D-2PA of the probe (<0.5%, which is at our noise limit). Pulsewidths from the picosecond OPG/OPA were measured by pump–probe and cross-correlation experiments to be 10–13 ps (FWHM), depending on the spectral region.

For the femtosecond gated detection experiments, we used a conventional PIN GaN detector with an active area of 0.25 mm^2 and a total GaN thickness of 5 μm, as determined using focused ion beam instrument (FEI 200 TEM FIB) cutting and imaging, with p- and i-GaN regions estimated to be <1 μm in thickness[36]. This detector was used in photoconductive mode, with a preamplifier gain factor of 40 (transimpedance gain, 400×10^3 V A^{-1}) and a variable reverse bias voltage from 1 to 4 V. Measurements of extreme ND-2PA in the GaN detector element resulted in cross-correlation of MIR (5.6 μm @ 0.5 GW cm^{-2}) pulses with near-UV (390 nm) pulses (Supplementary Fig. S1). The experimental results yielded ~230 fs (FWHM) for the MIR pulses, assuming Gaussian temporal profiles. The detector response voltage presented in Fig. 1a (390 nm + 5.6 μm curve) was recorded at zero time delay between the MIR and UV pulses. The detection of MIR pulses at 5.6 μm using gating pulses at 390 nm of different irradiances is presented in Fig. 1b. The background signal from D-2PA of the 390 nm pulses was eliminated by modulation of the weak MIR signal and the use of lock-in detection. The calculated D-2PA coefficient for 390 nm was ~2.2 cm GW^{-1}, which is more than two orders of magnitude less than the ND-2PA of ~240 cm GW^{-1}.

A conventional liquid-nitrogen-cooled HgCdTe (MCT) detector (Electro-Optical Systems Inc., model MCT14-040-E-LN6; active area, 16 mm^2, noise equivalent power (NEP) = 23×10^{-12} W $Hz^{-1/2}$, $D^* = 1.7 \times 10^{10}$ cm $Hz^{1/2}$ W^{-1}, $R = 7.8 \times 10^3$ V W^{-1} @ preamp out, pre-amp gain of 100, transimpedance gain 5×10^3 V A^{-1}) was used in the experiments for comparison. As discussed, for the case of non-degenerate gated detection, the signal is linearly proportional to the gate pulse irradiance $R = A \cdot I_g$, where $A_{IR\ gate} = 6.8 \times 10^{-11}$ cm^2 A W^{-2} and $A_{UV\ gate} = 7.1 \times 10^{-12}$ cm^2 A W^{-2}). As an example, the measured values are $R_{IR\ gate} = 0.034$ A W^{-1} for 0.5 GW cm^{-2} of 5.6 μm gate pulse irradiance, and $R_{UV\ gate} = 0.032$ A W^{-1} for 4.5 GW cm^{-2} of 390 nm gate pulse irradiance. Parameters used in the detection experiments and associated calculations[37–39] are given in Supplementary Table S1.

Received 4 April 2011; accepted 30 June 2011; published online 7 August 2011

References

1. Haque, S. A. & Nelson, J. Toward organic all-optical switching. *Science* **327,** 1466–1467 (2010).
2. Yumoto, J. *et al.* Enhancement of optical nonlinearity of heavy-metal oxide glasses by replacing lead and bismuth with thallium. *Appl. Phys. Lett.* **63,** 2630–2632 (1993).
3. Sasaki, F., Kobayashi, S. & Haraichi, S. Enhancement of the optical nonlinearity in pseudoisocyanine J aggregates embedded in distributed feedback microcavities. *Appl. Phys. Lett.* **81,** 391–393 (2002).
4. Soljačić, M. & Joannopoulos, J. D. Enhancement of non-linear effects using photonic crystals. *Nature Mater.* **3,** 211–219 (2004).
5. Hales, J. M. *et al.* Design of polymethine dyes with large third-order optical nonlinearities and loss figures of merit. *Science* **327,** 1485–1488 (2010).
6. Genevet, P. *et al.* Large enhancement of nonlinear optical phenomena by plasmonic nanocavity gratings. *Nano Lett.* **10,** 4880–4883 (2010).
7. Schuller, J. A. *et al.* Plasmonics for extreme light concentration and manipulation. *Nature Mater.* **9,** 193–204 (2010).
8. Capasso, F., Sirtori, C. & Cho, A. Y. Coupled quantum well semiconductors with giant electric field tunable nonlinear optical properties in the infrared. *IEEE J. Quantum Electron.* **30,** 1313–1326 (1994).
9. Paiella, R. *et al.* Self-mode-locking of quantum cascade lasers with giant ultrafast optical nonlinearities. *Science* **290,** 1739–1742 (2000).
10. Tanabe, T., Notomi, M., Kuramochi, E., Shinya, A. & Taniyama, H. Trapping and delaying photons for one nanosecond in an ultrasmall high-*Q* photonic crystal nanocavity. *Nature Photon.* **1,** 49–52 (2007).
11. Christodoulides, D., Khoo, I. C., Salamo, G. J., Stegeman, G. I. & Van Straland, E. W. Nonlinear refraction and absorption: mechanisms and magnitudes. *Adv. Opt. Photon.* **2,** 60–200 (2010).
12. Said, A. A. *et al.* Determination of bound-electronic and free-carrier nonlinearities in ZnSe, GaAs, CdTe, and ZnTe. *J. Opt. Soc. Am. B* **9,** 405–414 (1992).
13. Hutchings, D. C. & Van Stryland, E. W. Nondegenerate two-photon absorption in zinc blende semiconductors. *J. Opt. Soc. Am. B* **9,** 2065–2074 (1992).
14. Sheik-Bahae, M., Wang, J., DeSalvo, R., Hagan, D. J. & Van Styland, E. W. Measurement of nondegenerate nonlinearities using a two-color z scan. *Opt. Lett.* **17,** 258–260 (1992).
15. Sheik-Bahae, M., Hutchings, D. C., Hagan, D. J. & Van Stryland, E. W. Dispersion of bound electronic nonlinear refraction in solids. *IEEE J. Quantum Electron.* **27,** 1296–1309 (1991).
16. Wherrett, B. S. Scaling rules for multiphoton interband absorption in semiconductors. *J. Opt. Soc. Am. B* **1,** 67–72 (1984).
17. Olszak, P. D. *et al.* Spectral and temperature dependence of two-photon and free-carrier absorption in InSb. *Phys. Rev. B* **82,** 235207 (2010).
18. Hales, J. M. *et al.* Resonant enhancement of two-photon absorption in substituted fluorine molecules. *J. Chem. Phys.* **121,** 3152–3160 (2004).
19. Pati, S. K., Marks, T. J. & Ratner, M. A. Conformationally tuned large two-photon absorption cross sections in simple molecular chromophores. *J. Am. Chem. Soc.* **123,** 7287–7291 (2001).
20. Kogej, T. *et al.* Mechanisms for enhancement of two-photon absorption in donor–acceptor conjugated chromophores. *Chem. Phys. Lett.* **298,** 1–6 (1998).
21. Kleinman, D. A. & Boyd, G. D. Infrared detection by optical mixing. *J. Appl. Phys.* **40,** 546–566 (1969).
22. Gurski, T. R., Epps, H. W. & Maran, S. P. Upconversion of broadband infrared spectra. *Appl. Opt.* **17,** 1238–1242 (1978).
23. Watson, E. A. & Morris, G. M. Comparison of infrared upconversion methods for photon-limited imaging. *J. Appl. Phys.* **67,** 6075–6084 (1990).
24. Hadfield, R. H. Single-photon detectors for optical quantum information applications, *Nature Photon.* **3,** 696–705 (2009).
25. Gu, X. *et al.* Temporal and spectral control of single-photon frequency upconversion for pulsed radiation, *Appl. Phys. Lett.* **96,** 131111 (2010).
26. Thew, R. T., Zbinden, H. & Gisin, N. Tunable upconversion photon detector. *Appl. Phys. Lett.* **93,** 071104 (2008).
27. Urbach, F. The long-wavelength edge of photographic sensitivity and of the electronic absorption of solids. *Phys. Rev.* **92,** 1324 (1953).
28. Wu, J. & Luo, F. Ultrafast femtosecond all-optical modulation through nondegenerate two-photon absorption in silicon-on-insulator waveguides. *J. Russian Laser Res.* **29,** 490–496 (2008).
29. Vahala, K. J. Optical microcavities. *Nature* **424,** 839–846 (2003).
30. Leuthold, J., Koos, C. & Freude, W. Nonlinear silicon photonics. *Nature Photon.* **4,** 535–544 (2010).
31. Apiratikul, P. & Murphy, T. E. Background-suppressed ultrafast optical sampling using nondegenerate two-photon absorption in a GaAs photodiode. *IEEE Photon. Technol. Lett.* **22,** 212–214 (2010).
32. Boitier, F., Dherbecourt, J. B., Godard, A. & Rosencher, E. Infrared quantum counting by nondegenerate two photon conductivity in GaAs. *Appl. Phys. Lett.* **94,** 081112 (2009).
33. Hayat, A., Ginzburg, P. & Orenstein, M. Infrared single-photon detection by two-photon absorption in silicon. *Phys. Rev. B* **77,** 125219 (2008).
34. Hayat, A., Ginzburg, P. & Orenstein, M. Observation of two-photon emission from semiconductors. *Nature Photon.* **2,** 238–241 (2008).
35. Delfyett, P. J. Optical frequency combs from semiconductor lasers and applications in ultrawideband signal processing and communications. *J. Lightwave Technol.* **24,** 2701–2719 (2006).
36. Chow, P. P. *et al.* Group III—nitride materials for ultraviolet detection applications. *SPIE: Optoelectronics Conference Proceedings*, 3948–32 (2000).

37. Pugh, S. K., Dugdale, D. J., Brand, S. & Abram, R. A. Electronic structure calculations on nitride semiconductors. *Semicond. Sci. Technol.* **14,** 23–31 (1999).
38. Bass, M., Li, G. & Van Stryland, E. W. *Handbook of Optics: Volume 4, Optical Properties of Materials, Nonlinear Optics, Quantum Optics* 3rd edn (McGraw-Hill, 2010).
39. Sheik-Bahae, M., Hutchings, D. C., Hagan, D. J. & Van Stryland, E. W. Dispersion of bound electronic nonlinear refraction in solids. *IEEE J. Quantum Electron.* **27,** 1296–1309 (1991).

Acknowledgements

This work was supported in part by the US Army Research Office (grant no. 50372-CH-MUR) and the DARPA ZOE program (grant no. W31R4Q-09-1-0012).

Author contributions

D.A.F., C.M.C., L.A.P. and S.W. conceived and performed the experiments. C.M.C and D.A.F. modelled the data and performed the theoretical analysis. M.M. designed and implemented the detection system. D.J.H. and E.W.V.S. suggested the basic concept of enhanced ND-2PA for experiments and applications. All authors contributed to the discussion of the results and writing the paper.

Additional information

The authors declare no competing financial interests. Supplementary information accompanies this paper at www.nature.com/naturephotonics. Reprints and permission information is available online at http://www.nature.com/reprints. Correspondence and requests for materials should be addressed to E.W.V.S.